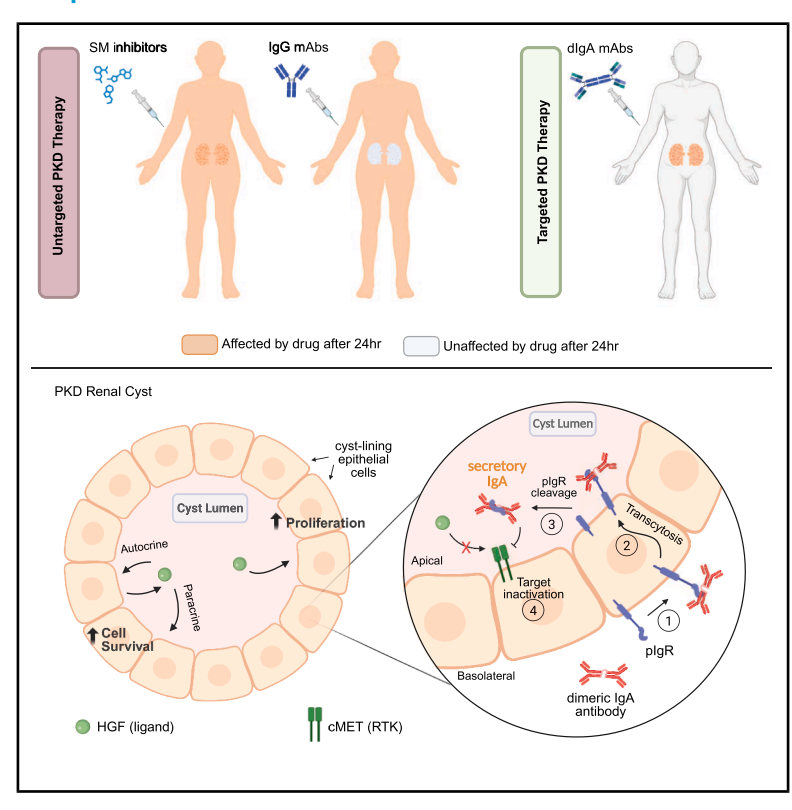


Development of a cyst-targeted therapy for polycystic kidney disease using an antagonistic dimeric IgA monoclonal antibody against cMET

Graphical abstract



Authors

Margaret F. Schimmel, Bryan C. Bourgeois, Alison K. Spindt, ..., Gavin E. Cornick, Yuqi Liu, Thomas Weimbs

Correspondence

weimbs@ucsb.edu

In brief

Current PKD therapies are limited by poor efficacy and off-target toxicity. Schimmel et al. show that recombinant dimeric IgAs can reach kidney cyst lumens and engage molecular targets to slow disease progression. This approach minimizes side effects and enables repurposing of validated IgG sequences for efficient delivery across epithelial barriers.

Highlights

- Dimeric IgA accumulated specifically in renal cysts at therapeutic concentrations
- cMET-dlgA treatment slowed cyst growth and improved kidney function in PKD mice
- Potent dlgA targeting identified cMET as a key pro-survival factor in PKD cysts
- dlgA offers a versatile platform to repurpose validated mAbs for mucosal diseases







Article

Development of a cyst-targeted therapy for polycystic kidney disease using an antagonistic dimeric IgA monoclonal antibody against cMET

Margaret F. Schimmel, Bryan C. Bourgeois, Alison K. Spindt, Sage A. Patel, Tiffany Chin, Gavin E. Cornick, Yuqi Liu, and Thomas Weimbs 1,2,*

¹Department of Molecular, Cellular, and Developmental Biology, University of California, Santa Barbara, Santa Barbara, CA 93106, USA ²Lead contact

*Correspondence: weimbs@ucsb.edu https://doi.org/10.1016/j.xcrm.2025.102335

SUMMARY

Polycystic kidney disease (PKD) is characterized by the development of fluid-filled kidney cysts and relent-less progression to renal failure. Current treatments have adverse effects and limited efficacy, enhancing the need for improved therapeutics. Here, we provide a proof of concept for the use of dimeric immunoglobulin A (IgA) (dIgA) monoclonal antibodies (mAbs) to target epithelial-enclosed cysts, by exploiting their ability to transcytose via the polymeric immunoglobulin receptor highly expressed on renal cyst-lining cells. We engineered an antagonistic dIgA mAb against the cell mesenchymal-epithelial transition (cMET) receptor, a driver of cyst progression, and demonstrated its specific binding and inhibition of cMET *in vitro*. *In vivo* studies in PKD rodent models showed efficient targeting of the mAb to renal cyst lumens and its ability to slow disease progression without apparent adverse effects. This study presents an intriguing avenue for developing antibody-based therapies for PKD and similar diseases by repurposing existing immunoglobulin G (IgG) mAbs into dIgA mAbs for superior targeting to epithelial-enclosed compartments.

INTRODUCTION

Over 12 million people worldwide suffer from autosomal dominant polycystic kidney disease (ADPKD or PKD), which results from a mutation in either the polycystin-1 (PC1) or polycystin-2 (PC2) gene. 1,2 These mutations cause tubular epithelial cell proliferation and growth of fluid-filled cysts throughout the kidneys that destroy healthy tissue over time in a process involving inflammation and fibrosis. The adverse effects, as well as the limited efficacy and patient availability of tolvaptan,³ the only approved drug for PKD,4 necessitates the development of improved therapeutics. There is no shortage of "promising" molecular drug targets for the treatment of PKD as dozens of pathways and proteins have been identified as drivers of PKD progression.⁵ In fact, many of these proteins can already be targeted with existing or novel small molecule (SM) drugs. The primary obstacle, however, is that virtually all of the potential drug targets implicated in PKD are widely expressed and serve important functions in many extra-renal tissues. SM drugs that affect PKD targets may be effective in inhibiting renal cyst growth, but they also tend to cause adverse effects in both the kidneys and extra-renal tissues that would be prohibitive for extended use in clinical practice.

A major advantage of monoclonal antibodies (mAbs), compared to SM drugs, is their typically higher target specificity, which greatly reduces or eliminates off-target adverse effects.^{6,7} The lack of oral bioavailability of mAbs is partially overcome by

the much longer half-lives of mAbs compared to SM drugs. However, to our knowledge, no mAb with reported efficacy in PKD animal models has progressed to clinical studies. A likely explanation for these translational failures is that many of the growth factors/receptors and cytokines that are implicated in PKD and could be targeted with mAbs are localized to the luminal compartment of the enclosed, epithelial-lined renal cysts.⁵ Any growth factors secreted into the cyst fluid (CF) could cause persistent auto- and paracrine activation by stimulating their cognate receptor on the apical membranes of cyst cells and could lead to an inescapable, permanent state of activation. The biopharmaceutical industry almost exclusively uses immunoglobulin (Ig)G isotypes to develop mAb therapeutics. However, this Ig isotype is not capable of crossing the epithelial barrier of renal cysts and therefore does not gain access to this compartment.8 Considering this problem, it is not surprising that mAbs in IgG format may be ineffective in PKD if the intended target resides in cyst lumens.

To overcome this problem, we have utilized antibodies of a different isotype, IgA, specifically dimeric IgA (dIgA). The purpose of dIgA in nature is to cross epithelial barriers for excretion into external secretions as a first line of defense against pathogens. This is accomplished through transcytosis via the polymeric immunoglobulin receptor (pIgR). pIgR binds polymeric Ig species, such as dIgA, at the basolateral side of epithelial cells and releases them into the apical space in a complex with the ectodomain of pIgR, ^{5,9,10} called secretory component (SC), to form





the final "secretory IgA" (sIgA). SC provides the dimeric antibody with increased stability and protection from proteases. ¹¹ We found that the pIgR is highly expressed on cyst-lining cells in human PKD and mouse models and is driven by the aberrant activation of the signal transducer and activator of transcription 6 pathway. ^{2,8,12} More recently, pIgR peptides were found to be increased in urine from patients with ADPKD. ¹³ In a separate study, the elevated expression of pIgR in proximal tubules during kidney disease strongly correlated with the presence of urinary sIgA in human patients. ¹⁴ These studies support the translational relevance of this receptor to disease pathogenesis.

plgR can only transcytose dlgA unidirectionally into cyst lumens. As the majority of renal cysts have lost their connection to the tubular system, dlgA will become trapped there as a result. Importantly, due to the relatively short serum half-life of dlgA, 15,16 any remaining injected dlgA would be rapidly cleared systemically by secretion via the intestinal epithelium and bile. The net effect is that parenterally administered dlgA is specifically targeted to renal cyst lumens, unlike lgG mAbs, as we demonstrated previously, and would be expected to have minimal systemic effects or accumulation, unlike SM drugs.

In this study we investigate whether the progression of PKD can be affected by utilizing an antagonistic dlgA mAb against a luminal target protein. As the target, we chose the cell mesenchymal-epithelial transition (cMET) protein, a receptor tyrosine kinase (RTK) which has previously been implicated as a possible driver of cyst progression in PKD mouse models. 19,20 cMET is overexpressed in renal cysts and present on the apical membrane 19,20 where it may be readily activated by its ligand, 21 the hepatocyte growth factor (HGF). HGF has been shown to be highly expressed in cystic fluid. Furthermore, an SM cMET inhibitor was demonstrated to slow PKD progression in an embryonic PKD mouse model, 20 suggesting that it could be a valid therapeutic target.

We used the IgG variable domain of a previously described human/mouse-cross-reactive, inhibitory cMET antibody²² to engineer a function-blocking cMET mAb in dIgA format. We found that this antibody properly binds and inhibits its target *in vitro* and can be effectively transcytosed across a renal epithelial layer via pIgR. *In vivo*, specifically in mouse and rat models of PKD, this antibody targets to cyst lumens and inhibits disease progression in rapidly progressing disease models without any detected adverse effects. The work here has yielded proof of concept, as well as proof of efficacy for this cyst-targeted therapeutic approach to pharmacologically target some of the most impactful proteins in PKD that have already been discovered.

RESULTS

Engineering, expression, and purification of stable dlgA recombinant antibodies

To produce the recombinant dlgA molecule used in this study, antigen-binding variable chain region sequences from a previously described function-blocking cMET lgG antibody²² were cloned into separate heavy-chain (HC) and light-chain (LC) plasmids containing their respective human lgA₁ constant regions (Figures 1A and 1B). The recombined HC and LC plasmids

were then co-expressed in HEK293F cells along with joining chain (JC) plasmid containing Myc and $6\times$ histidine (His) tags to assist in purification and specific detection (Figure 1B). Small-scale expression experiments were conducted to confirm proper sizes of each chain and to optimize the molar transfection ratio that would yield the highest amount of dlgA species (Figure 1C). An HC:LC:JC molar ratio of 1:2:3 was used for the remainder of production based on these experiments. Crude supernatants (SNs) contained the antibody in monomeric (mlgA), dimeric (dlgA), and polymeric (plgA) forms (Figure 1C). The concentrated, crude SN was first purified with immobilized metal affinity chromatography utilizing the $6\times$ His tag on the JC to capture dlgA and remove mlgA, followed by anion exchange chromatography to yield highly purified and concentrated dlgA suitable for *in vivo* studies (Figures 1D and 1E).

The cMET antigen-binding sequences were initially engineered onto a mouse IgA backbone; however, the resulting, purified mouse dIgA was difficult to detect *in vivo*. To investigate this, the mouse cMET-dIgA and its human dIgA1 counterpart were incubated at 37°C for 24 h in either PBS or CF collected from PKD mice. The mouse dIgA was much less stable in CF than the human dIgA1 and began degrading as early as 8 h (Figure 1F). This difference is most likely due to the unique tail-piece region present on the HC of human IgA1 that confers enhanced stability. ¹¹ Thus, the remainder of the study was conducted using the cMET-dIgA on a human IgA1 backbone.

In vitro functional testing of cMET-dlgA

To confirm specific target binding of our cMET-dlgA, Chinese hamster ovary (CHO) cells grown on coverslips were transfected with either human, mouse, or rat cMET plasmids. The source antibody used for engineering our dlgA was reported to react with both human and mouse cMET.²² Indeed, our cMET-dlgA bound to both species of its native target protein, as well as to native rat cMET, which was apparent through colocalization of a commercial cMET IgG antibody with our cMET-dlgA (Figure 2A). The antagonistic ability of our cMET-dlgA was tested in mouse collecting duct cells that endogenously express cMET and its intracellular signaling pathway. Following HGF stimulation, cMET-dlgA treatment blocked cMET phosphorylation in cells, as well as p-ERK1/2 and p-Akt signals in a dose-dependent manner (Figure 2B). In some cases, the dlgA reduced phosphorylation to levels lower than-or comparable to-a cMET competitive SM inhibitor, capmatinib (Figure 2B). This was also true when the cMET-dlgA was functionally tested in HeLa cells expressing human cMET endogenously (Figure S1). Quantification of p-cMET immunoblot intensity resulted in estimation of the half-maximal inhibitory concentration (relative IC50) of 1.8 nM (\sim 0.5 μ g/mL) for the cMET-dlgA (Figure 2B). No agonist activity occurred in mouse or human cells at any dose of dlgA tested in the absence of HGF (Figures 2B and S1), indicating that the mAb was not inducing RTK dimerization and activation as has been reported for some antagonistic cMET IgGs.^{23,24}

Transcytosis assays were performed in transwell systems using the renal epithelial Madin-Darby canine kidney (MDCK) cell line, which stably expresses plgR, to determine if the recombinant dlgA molecule can be properly trafficked across an epithelial barrier. When the cMET-dlgA was applied to the

Article



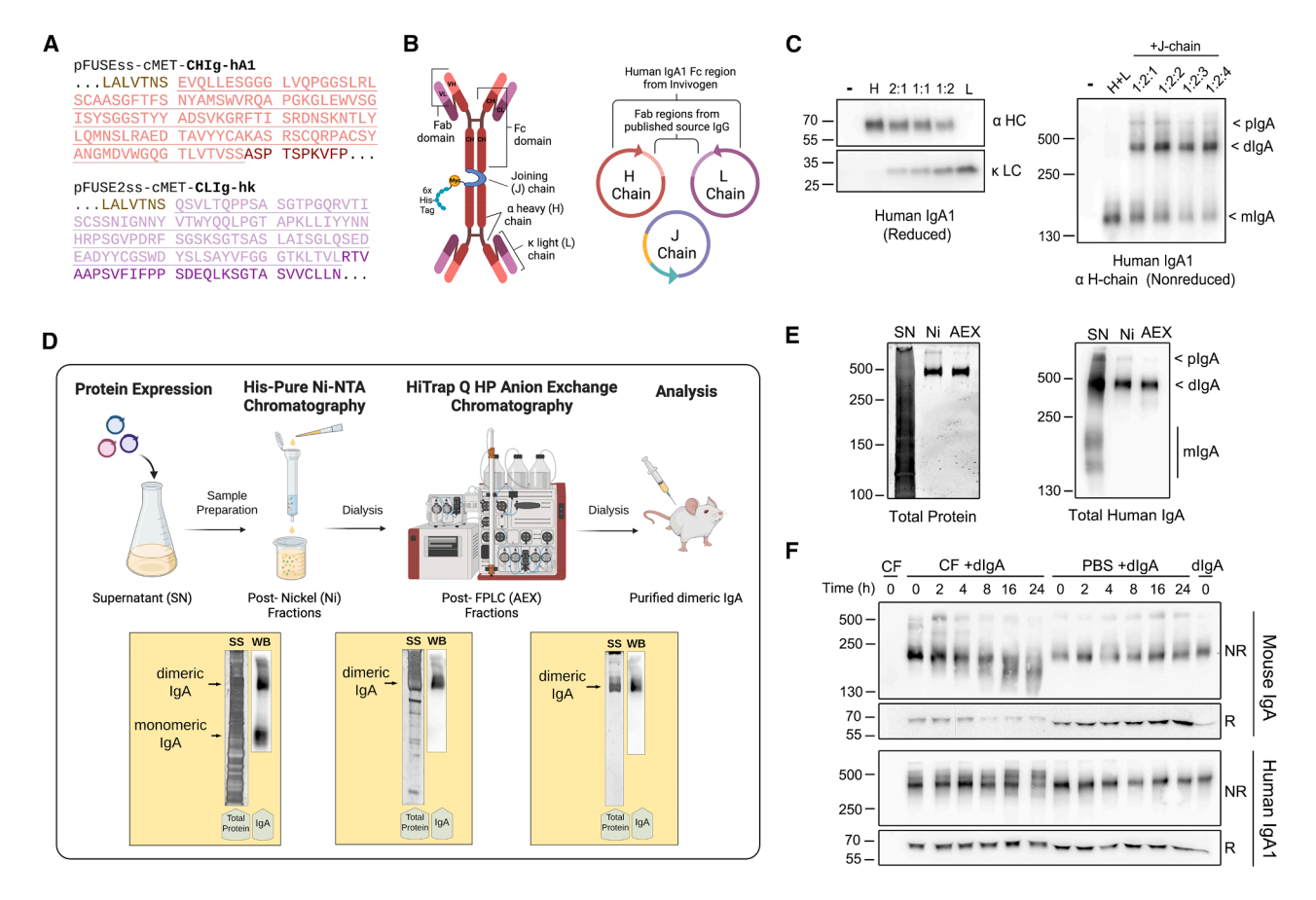


Figure 1. Recombinant engineering and high-yield production of human dimeric IgA1 monoclonal antibodies

(A and B) Recombinant cloning utilized (A) amino acid sequences of the human IgA1 antigen-binding (Fab) domains shown in light red (heavy chain) or purple (light chain), in frame with the IgA1 constant domain sequences shown in dark red or purple to produce (B) recombinant human dimeric IgA mAbs.

(C) Various molar ratios of heavy (H), light (L), and joining (J) chain were transiently transfected in 293F cells. Cell pellets were lysed in SDS and run on a reducing immunoblot to confirm individual chain molecular weights. Cell supernatants were run on a nonreducing immunblot to visualize dimer formation.

(D) dlgA production workflow. Samples collected after each step of purification are analyzed for total protein contaminants via silver stain as well as for human IgA specifically via immunoblot under nonreducing conditions, shown in yellow shaded boxes.

(E) Samples from each step of purification loaded side by side. SN, cell culture supernatant; Ni, post-nickel purification; AEX, anion exchange chromatography. Polymeric (plgA), dimeric (dlgA), and monomeric (mlgA) species can be seen after specific staining for human lgA1.

(F) Recombinant mouse and human IgA samples were analyzed via immunoblot after *in vitro* incubation in CF or PBS (pH 7.4). Dimer stability was visualized under nonreducing (NR) conditions while separated alpha heavy chains under reducing (R) conditions.

basolateral side of these polarized cells, it was transported to the apical (luminal) compartment. After 24 h, significant accumulation of the antibody was observed in the apical chamber (Figure 2C). The observed size shift of apical dlgA sample compared to the dlgA control lane indicates the addition of the plgR ectodomain (SC) during transcytosis. MCDK cells lacking plgR failed to transcytose cMET-dlgA (Figure 2C). We have previously reported that MDCK cells lose cell junctions when grown in calcium-depleted media and establish their apical membrane in the form of intracellular vesicular apical compartments (VACs). These VACs can then become the destination for plgR-mediated trafficking.²⁵ Under low Ca²⁺ conditions, the cMET-dlgA, added to the cell culture media, was endocytosed and trafficked into VACs of MDCK cells stably expressing plgR, but not in cells lacking plgR (Figure 2D). These analyses together demonstrated that our method of reformatting and engineering dlgA mAbs preserves the normal function of both the Fab region to bind cMET and the Fc region to allow for plgR-mediated transcytosis.

cMET-dlgA renal cyst targeting in an adult PKD rat model

We previously characterized plgR expression and dlgA renal targeting in juvenile and adult PKD mouse models. To extend these data, we now characterized a rat model, the well-established, non-orthologous Sprague-Dawley Han rat (Han:SPRD Cy/+) model, which has been commonly used to assess the efficacy of PKD therapies. Similar to our previous reports in PKD mouse models, plgR expression is strongly upregulated in polycystic kidneys of 12 week-old adult Cy/+ rats compared to wild-type controls (Figure 3A). In agreement with the localization of plgR in human PKD, 8,14 plgR was expressed primarily in cysts originating from aquaporin 1-positive (AQP1+) proximal



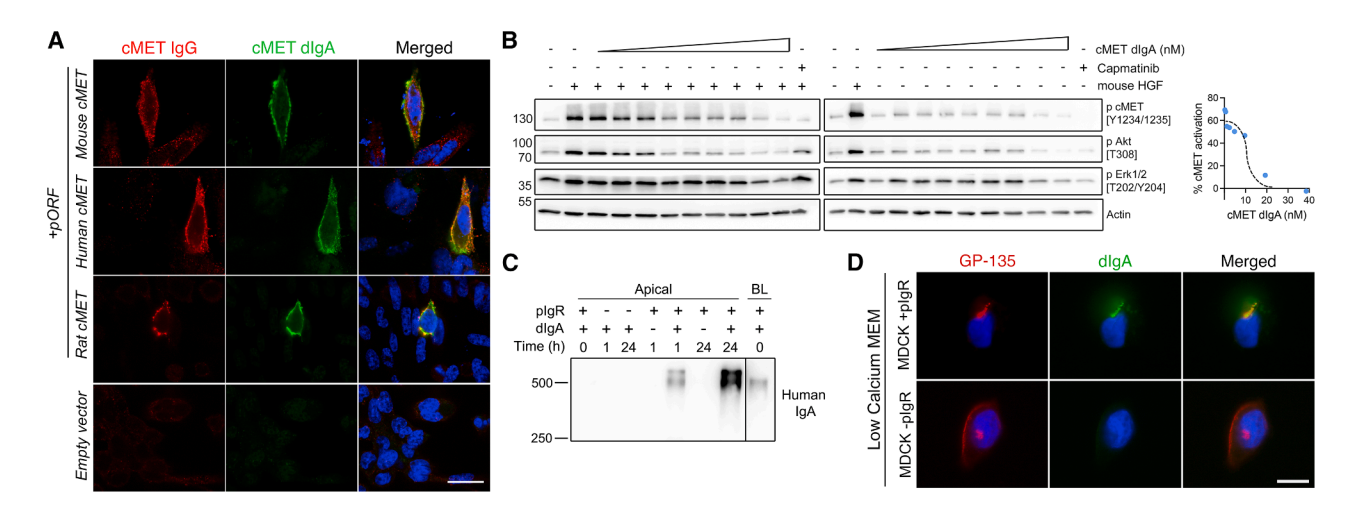


Figure 2. Recombinant cMET-dlgA displays potent antagonist activity and retains the ability to transcytose via plgR

(A) cMET-dlgA specifically bound mouse (top row), human (2nd row), and rat (3rd row) cMET in transiently transfected CHO cells. An empty DNA vector (bottom row) was used for control. Human dlgA (used as a primary detection antibody, green); cMET (commercial lgG specific for all 3 species, red); DAPI (blue). Scale bar, 20μM.

(B) cMET-dlgA blocked endogenous cMET receptor activation in mouse IMCD-3 cells after HGF stimulation (left panels) and did not cause receptor dimerization in the absence of HGF (right panels). Capmatinib (cMET SM inhibitor) was used as a negative control. Cells were lysed in SDS and analyzed via immunoblot. Quantification of immunoblot signal intensity from +HGF/+dlgA samples was performed using Image Studio Lite, normalized to actin. See also Figure S1.

(C) Transcytosis of cMET-dlgA visualized via immunoblot of human IgA in apical or basolateral (BL) media samples from MDCK cells (with/without plgR stably transfected). All samples were run under nonreducing conditions. A vertical line between lanes indicates that the two sections of the blot were adjusted separately on Photoshop to improve visibility.

(D) Transcytosis into apical compartments also occurred under low-calcium conditions in MDCK cells expressing plgR. GP-135 (apical membrane marker, red); human dlgA (used as a primary detection antibody, green); DAPI (blue). Scale bar, 10 µM.

tubules in these rats (Figure 3B). A single-injection study was performed in this model to investigate the renal distribution of the cMET-dlgA. 24 h after intraperitoneal (i.p.) injection of 1 mg cMET-dlgA (~3 mg/kg), the mAb could be recovered in aspirated renal CF (Figure 3C). The observed size shift of the recovered antibody indicated that the SC was attached, further demonstrating that it had indeed reached cyst lumens by transcytosis via plgR (Figure 3C).

The level of total cMET protein on cyst-lining cells was visibly reduced 24 h after the single cMET-dlgA injection (Figure 3D), most notably in AQP1+ cysts where the mAb presumably targeted via upregulated plgR. Activation of cMET, as indicated by the expression of phosphorylated cMET, was also blunted or strongly reduced in cortical cysts compared to control-injected rats (Figure 3D). Cysts in dlgA-injected rats also harbored fewer epithelial cells positive for the cell-cycle marker Ki67 compared to control rats. In contrast, Ki67 was not impacted in healthy tissue surrounding the cysts (Figure 3E). Altogether, these results indicate that parenterally administered cMET-dlgA antibody undergoes plgR-mediated transcytosis into renal cyst lumens where it potently blocks cMET activation and downstream cell proliferation.

cMET-dlgA renal cyst targeting in an early-onset PKD mouse model

We previously reported that non-specific human dlgA administered via i.p. injection in PKD mouse models, including the non-orthologous BALB/c polycystic kidney (Bpk) model, is targeted to polycystic kidneys and accumulates in renal CF after

24 h.8 To investigate the pharmacokinetics of our cMET-dlgA antibody in mice, we utilized the Bpk model harboring homozygous mutations in the Bicc1 gene, and conducted single-injection experiments. We first confirmed that plgR is upregulated in these mice compared to wild-type mice (Figure 4A), as was seen previously.8 After single i.p. injection of 20 mg/kg cMETdlgA, approximately 10% of injected mAb were recoverable in CF after 24 h, and \sim 5%–7% were retained in CF after 3 days (Figures 4B and 4C). As expected, much smaller amounts of cMET-dlgA were found in kidneys that had been depleted of CF (Figure 4B) or in wild-type kidney tissue (Figure S2) after a single injection in Bpk or WT mice, respectively. This strongly supports the model that retention of dlgA is specific to renal cysts and that levels of dlgA can reach therapeutically relevant concentrations in CF. Comparing the size of the injected dlgA antibody side by side between serum, depleted kidney, and CF samples suggests attachment of SC in CF that was not present on un-injected cMET-dlgA (Figure 4D). The presence of SC on the recovered mAb was confirmed by nickel precipitation of the His-tagged JC out of collected CF, followed by detection with an SC-specific antibody (Figure 4E). We further confirmed cyst targeting through visualization of the injected cMET-dlgA inside renal cyst lumens of injected Bpk mice. A human-specific antihuman IgA antibody detected no signal in vehicle control-injected Bpk mice (Figure 4F), ruling out non-specific binding of the detection antibody to endogenous mouse dlgA, which is present in CF of Bpk mice.8 In contrast, mice injected with the cMET-dlgA showed robust signal along the apical plasma membranes of cyst-lining epithelial cells and to apparent luminal cell

Article



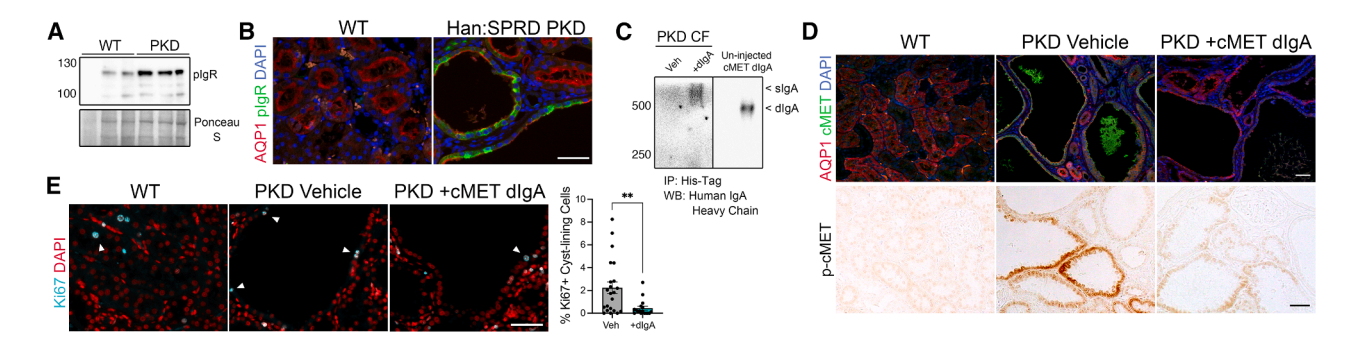


Figure 3. cMET-dlgA traffics to PKD Han rat cysts and downregulates cMET signaling in cyst-lining cells

(A and B) Untreated PKD Han:SPRD adult male rats upregulate plgR expression compared to WT as seen in (A) immunoblot of whole kidney lysates, n = 3, as well as (B) paraffin-embedded kidney sections stained by immunofluorescence for plgR (green), AQP1 (red), and DAPI (blue). Rats were injected with a single dose of 1 mg cMET-dlgA and sacrificed 24 h later, n = 5.

(C) Immunoprecipitation of CF using nitrilotriacetic acid (NTA)-nickel (Ni) ion resin followed by immunoblot specific for human IgA1 revealed secretory IgA (slgA) recovery. Un-injected purified dimeric IgA (dlgA) was loaded for size comparison. A vertical line between lanes indicates that the two sections of the blot were adjusted separately on Photoshop to improve visibility.

(D) Immunofluorescent staining of C-terminal cMET (red), AQP1 (red), and DAPI (blue), as well as immunohistochemistry staining of phospho-cMET, decreased after dlqA administration.

(E) Immunofluorescent staining of Ki67 (cyan) and DAPI (red) showed the most significant decrease in cyst-lining cells (white arrowheads), with quantification of the fraction of Ki67+ nuclei in a cyst. Each point on the graph represents that percentage for a single cyst in a given field.

All image scale bars, 100 µm. Statistical analyses were performed using Mann-Whitney unpaired one-tailed t test and represented as mean ± SEM. A p value of less than 0.05 was considered significant.

debris (Figure 4F). This suggests that the cMET-dlgA antibody was successfully transcytosed into cysts, where it bound to its target protein on these membranes. Together, it can be concluded that the parenterally administered cMET-dlgA antibody efficiently targets to renal cyst lumens through plgR-mediated transcytosis in the Bpk mouse model and can remain trapped in that space for 3 days or more.

Short-term cMET-dlgA treatment in a non-orthologous PKD mouse model

The cMET ligand HGF acts via paracrine signaling to promote proliferation, survival, invasion, and metastasis in tumor cells^{29,30} by activation of downstream pathways such as the extracellular signal-regulated kinase (ERK/mitogen-activated protein kinase).4 It was reported that reduced ubiquitination of cMET in PKD causes the receptor to accumulate on perinuclear vesicles, leading to prolonged pro-proliferative signaling.²⁰ To investigate the potential efficacy of our cMETdlgA antibody after its delivery to renal cyst lumens, we treated juvenile Bpk and wild-type mice with 20 mg/kg/day cMET-dlgA or with vehicle control for 1 week (Figure 5A). The expression level of cMET, including its intracellular accumulation and presence on the apical membrane, significantly decreased in cyst-lining cells in Bpk mice after cMET-dlgA treatment (Figures 5B and 5C). This suggests that cMET-dlgA treatment may be causing cMET ectodomain shedding³¹ and/or receptor internalization and degradation-both of which would antagonize HGF-mediated receptor signaling specifically in cyst cells. CF from proximal tubules has been reported to contain the highest levels of HGF compared to other cysts. 19,32 The significant decrease of cMET receptor expression in Lotus tetragonolobus lectin-positive proximal cysts (Figure 5B) indicates that HGF signaling is inhibited as a result of cMET-dlgA-mediated receptor downregulation. In support of this, cMET-dlgA treatment led to a robust decrease in p-cMET signal in cyst-lining cells compared to controls (Figure 5D) as well as potent downregulation of p-ERK signaling, a downstream pathway of cMET, in cyst-lining epithelial cells (Figures 5E and 5F). Costaining for human IgA identified renal cysts containing the cMET-dlgA antibody, and these cysts completely lacked detectable p-ERK signal (Figure 5E). cMET-dlgA treatment also led to increased phosphorylation of the AMP-regulated kinase (AMPK) in tubular and cystic epithelial cells (Figure 5G), suggesting enhanced homeostatic regulation in these kidnevs relative to vehicle-treated animals through activation of this critical cellular energy sensor. Altogether, these results show that 1-week treatment of Bpk mice with this dlgA antibody inhibits cMET activity in renal cysts. This, in turn, downregulates cell growth signals and potentially allows the cells to return to a more regulated metabolic state in this mouse model.

Although cystogenesis begins in utero³³ and progresses rapidly in the Bpk model, 1 week of cMET-dlgA treatment beginning at post-natal day (P)7 was sufficient to slow cyst expansion compared to vehicle-treated mice (Figures 6A and 6B). The preservation of healthy renal tissue was evident through thicker parenchyma seen in the treated kidneys (Figures 6A and 6B). The renal cystic index decreased in cMET-dlgA-treated mice (Figure 6C), with the most significant reduction observed in the kidney cortex where the majority of proximal cysts are located (Figure 6D). The two-kidney-to-body weight ratios (Figure 6E) significantly decreased in cMET-dlgA-treated mice compared to vehicle-treated mice indicating overall inhibition of renal growth. Serum creatinine levels were also significantly decreased in cMET-dlgA-treated mice compared to vehicletreated (Figure 6F) mice indicating better preservation of renal function. Cyst-lining cells from cMET-dlgA-treated mice



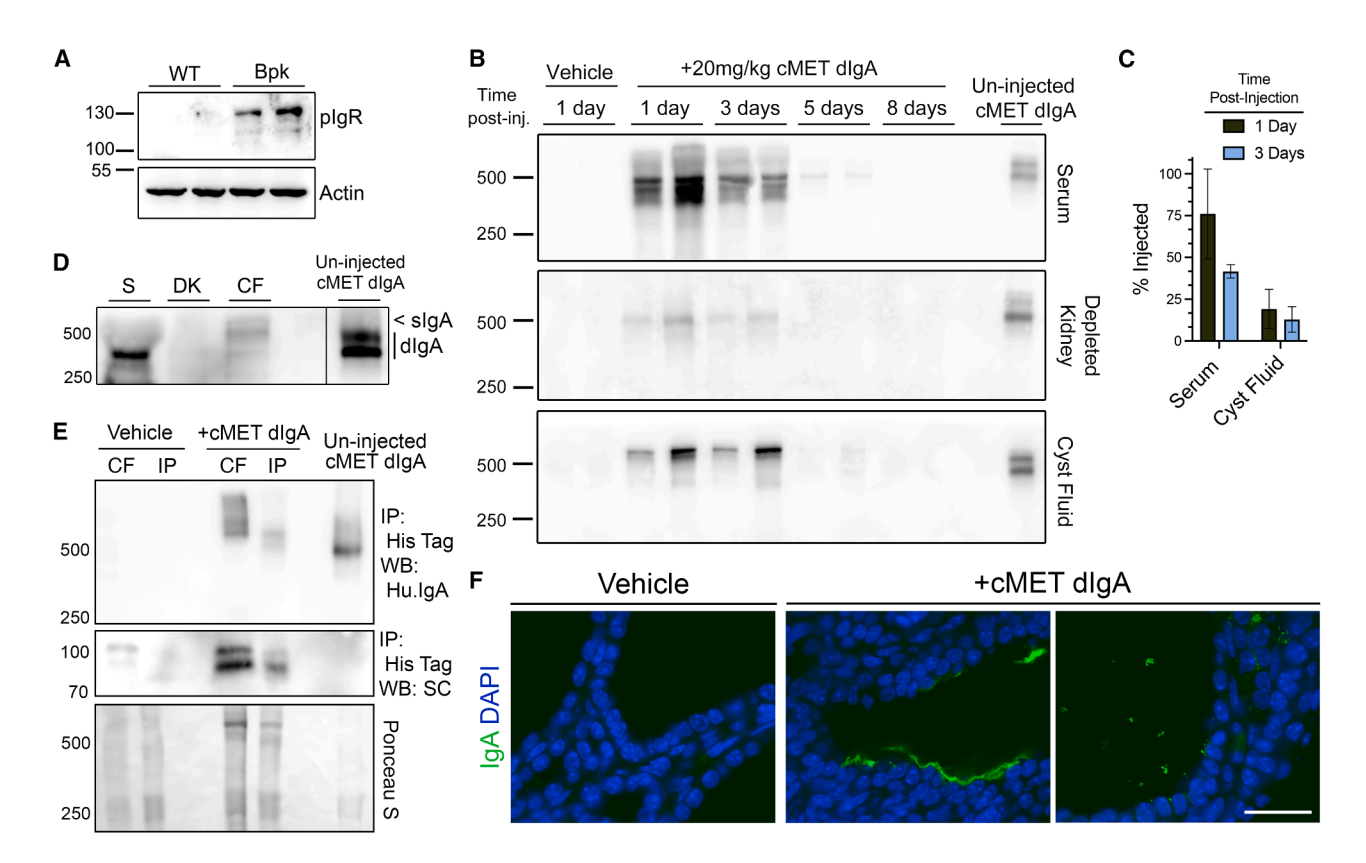


Figure 4. cMET-dlgA accumulates and stabilizes in Bpk mouse cyst lumen via plgR-mediated transport

(A) Untreated Bpk mice, P14, upregulate plgR expression in whole kidney lysates compared to age-matched WT mice.

(B) Serum (S), CF-depleted kidneys (DKs), and cyst fluid (CF) from Juvenile Bpk mice were analyzed 1, 3, 5, and 8 days post-dlgA injection. Sample concentrations were equalized via spectrophotometry. See also Figure S2.

(C) Recovery of dlgA in serum and CF was quantified 1 and 3 days post-injection via sandwich ELISA. Triplicate values from each +dlgA timepoint group (n = 2) was plotted from CF or serum and represented as mean ± SEM.

(D) Side-by-side comparison of these samples on a nonreducing SDS-PAGE gel.

(E) Immunoprecipitation of CF using NTA-Ni resin and antibodies specific for either human IgA1 (nonreduced) or secretory component (SC) (reduced). Un-injected cMET-dIgA was loaded on all immunoblots for size comparison of dimeric (d) and secretory (s) IgA. A vertical line between lanes indicates that the two sections of the blot were adjusted separately on Photoshop to improve visibility.

(F) Immunofluorescent staining of human IgA (green) and DAPI (blue) shows targeting of cMET-dIgA to renal cyst lumen. Scale bar, 100 μm.

exhibited a significant decrease in the ratio of proliferating cyst-lining cells, often reaching levels comparable to those in wild-type kidney tubule cells (Figure 6G). Most notably, cMET-dlgA treatment appears to have triggered a dramatic onset of apoptosis specifically in cyst epithelial cells, but not in healthy renal tissue (Figure 6H). No changes in body weight (Figure 6I) or lung-to-body weight ratios (Figure 6J) were observed, nor any other apparent changes that could suggest off-target effects, in cystic or in wild-type control mice. Altogether, these results serve as proof of therapeutic efficacy for this approach and further validate the cMET pathway as a driver of PKD disease progression and a viable drug target.

Short-term cMET-dlgA treatment in an orthologous Pkd1 mouse model

In order to validate the therapeutic potential of our dlgA approach in an ADPKD orthologous rodent model, we utilized a Pkd1^{fl/fl} tamoxifen-inducible mouse model. Similar models have been described to have a developmental switch that dic-

tates the onset of the disease: induction of Pkd1 deletion after P12–P14 results in slow cyst development over months whereas deletion before P12–P14 results in rapid cyst progression as early as 3 weeks post-induction.³⁴ The timing of tamoxifen induction used here led to development of a moderate-severe cystic phenotype at 3–5 weeks post-induction. During this time frame, cystic progression is not as variable as in the Bpk model and allows for feasible pharmacological studies that may be more predictive for human ADPKD.

Pkd1^{fl/fl} mice were treated with either 10 mg/kg cMET-dlgA or vehicle every other day for 2 weeks (Figure 7A) to assess efficacy. As was seen in the Bpk model, dlgA treatment reduced cMET receptor expression and induced apoptosis specifically in cyst-lining cells, but not in healthy interstitial tissue (Figures 7B–7D). Phospho-cMET was reduced in cyst-lining cells of these kidneys as well as in whole kidney lysates along with *p*-Src and *p*-ERK to a lesser degree (Figure S3). Off-target induction of apoptosis or cMET pathway inhibition was not observed in the small intestines of dlgA-treated mice (Figure S4),





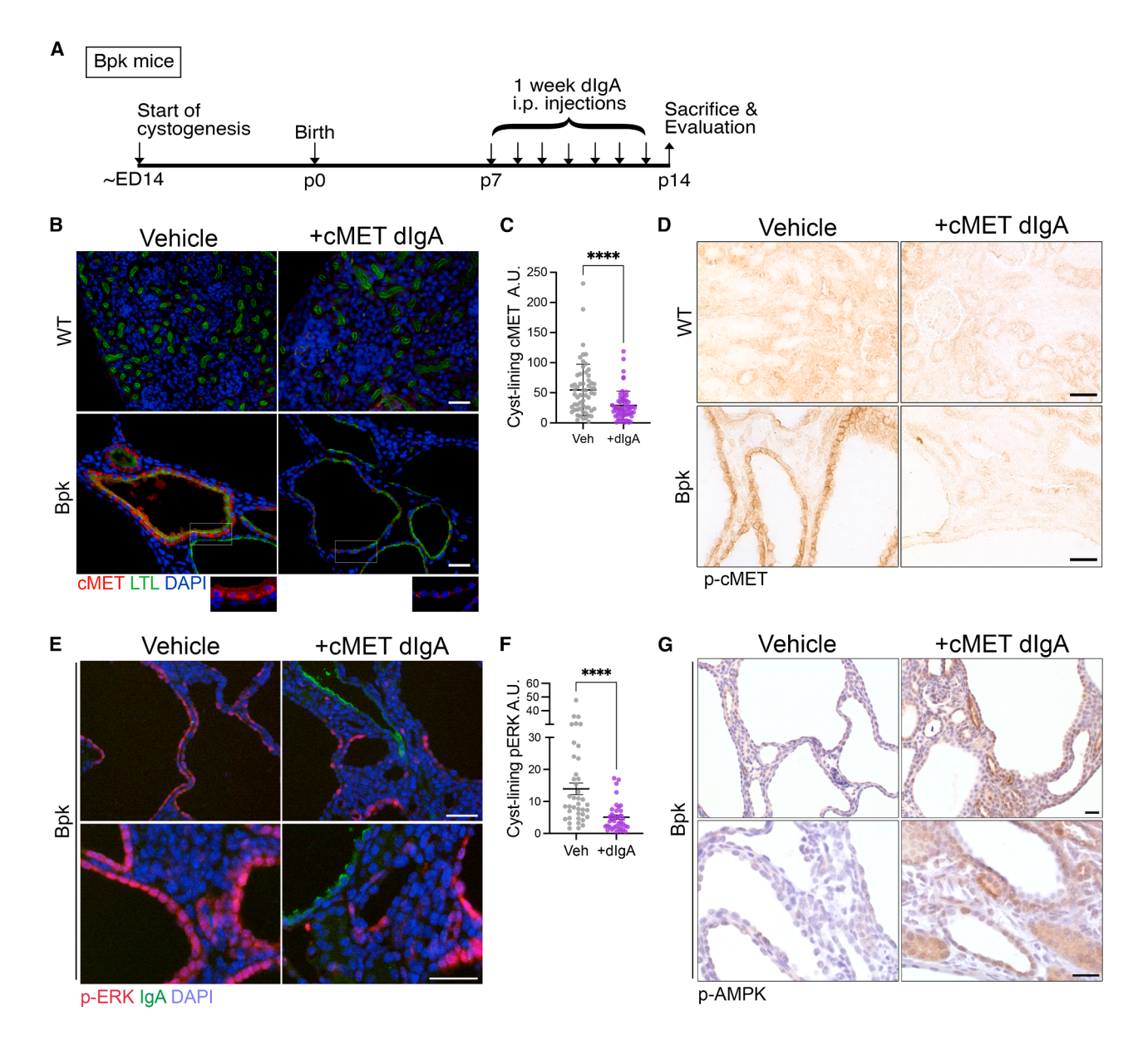


Figure 5. cMET-dlgA treatment causes potent target pathway inhibition in rapid-onset Bpk mouse model

(A) Short-term treatment timeline in Bpk model that begins cystogenesis *in utero* (ED). WT and Bpk mice were injected with 20 mg/kg/day cMET-dlgA or vehicle for 1 week starting at post-natal day (P)7. Analysis of kidney sections from these mice included (B) immunofluorescent staining for total cMET (red), proximal tubules stained with LTL (*Lotus tetragonolobus* lectin) marker (green), and DAPI (blue); (C) quantification of total cMET from (B) in cyst-lining cells; (D) immunohistochemistry stain of phospho-cMET; (E) immunofluorescent staining for phospho-ERK1/2 (red), human IgA (green), and DAPI (blue); (F) quantification of phospho-ERK from (E) in cyst-lining cells; and (G) immunohistochemistry stain of phospho-AMPK. Nuclei were counterstained with hematoxylin. All image scale bars, $50 \,\mu$ m. Statistical analyses were performed using Mann-Whitney unpaired one-tailed t test and represented as mean \pm SEM. A ρ value of less than 0.05 was considered significant.

supporting the proposed mechanism of action and safety of this dlgA approach.

dlgA-treated mice had notably denser tissue morphology (Figure 7E), mainly in the cortex and along the cortical-medullary junction. While there was no reduction in total kidney weight as a fraction of body weight following 2 weeks of treatment (Figure 7F), these mice had significantly decreased cyst areas throughout the kidney (Figure 7G). A significant reduction in fibrosis surrounding the cysts of these mice was found

(Figure 7H), yet no effect on collagen abundance in the small intestines was found (Figure S4).

Serum creatinine (Figure 7I) and blood urea nitrogen (BUN; Figure 7J) levels following cMET-dlgA treatment were significantly decreased compared to control indicating better preservation of renal function after just 2 weeks. With regard to extra-renal effects, dlgA treatment appears to have somewhat alleviated the minor cardiac atrophy that occurred after Pkd1 deletion in vehicle-treated mice, yet not to a



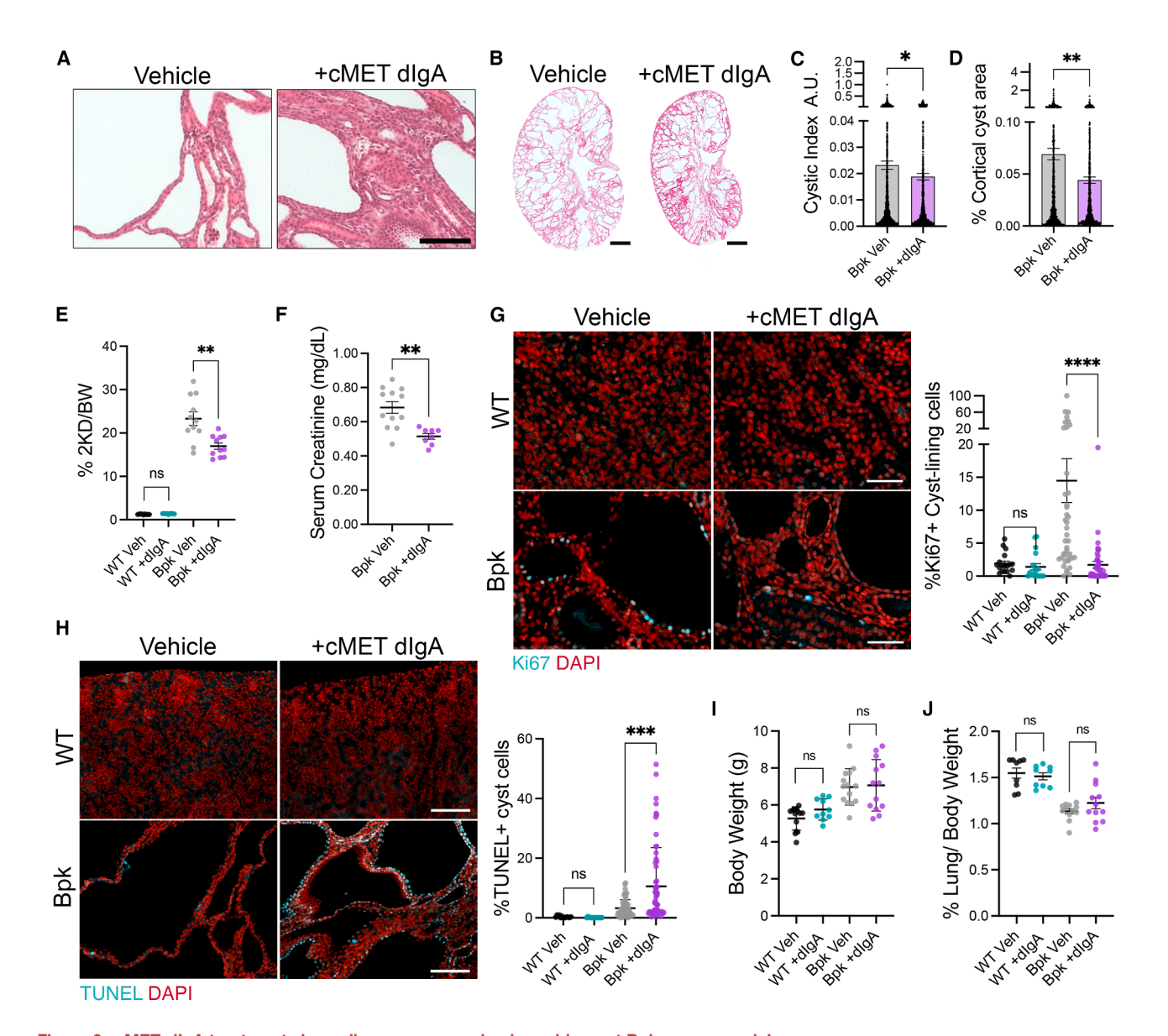


Figure 6. cMET-dlgA treatment slows disease progression in rapid-onset Bpk mouse model

 $\label{eq:hamiltonian} \mbox{H\&E stain of Bpk kidney sections after 1 week of daily i.p cMET-dlgA or vehicle injections.}$

(A–F) (A) Representative images, scale bar = 100 µm, and (B) stitched composite images, scale bar, 1 mm. Quantification of (C) cystic index by Photoshop grid scoring, (D) cortical cyst area as a fraction of the total tissue area using ImageJ, (E) two-kidney-to-body weights (2K/BW) of mice from each group after treatment, and (F) creatinine concentrations in BPK serum samples using QuantiChrom creatinine assay kit.

(G-J) (G) Immunofluorescent staining for the proliferation marker, Ki67 (cyan) and DAPI (red); scale bar, $50 \mu m$; (H) TUNEL stain for apoptotic cells (cyan) and DAPI (red); scale bar, $100 \mu m$, with quantification of the fraction of Ki67+ or TUNEL+ nuclei in a Bpk cyst or in WT tubular epithelial cells. Each point on the graph represents that percentage for a single cyst or tubule in a given field. dlgA treatment had no significant effect on (I) body weight or (J) lung weight as a fraction of total body weight compared to vehicle treatment in WT or Bpk mice.

Statistical analyses were performed using Mann-Whitney unpaired one-tailed t test and represented as mean ± SEM. A p value of less than 0.05 was considered significant.

significant degree (Figure S4). There was no change in lung weight of dlgA- versus vehicle-treated mice (Figure S4), and no cMET-dlgA was detectable in lung tissue at the end of treatment (Figure 7K). In contrast, cMET-dlgA was abundant in CF 2 days after the final injection at approximately 1 μ g/mL (Figure 7K), which surpasses its predicted IC50 of \sim 0.5 μ g/mL. In contrast, cMET-dlgA was no longer detectable

in circulation suggesting that it would lack systemic effects (Figure 7K).

Overall, these results show that cMET-dlgA effectively targets to cysts in an orthologous PKD model where it blunts cMET signaling, thereby slowing cystic and fibrotic progression as well as the decline in renal function without any apparent extra-renal adverse effects.

Article



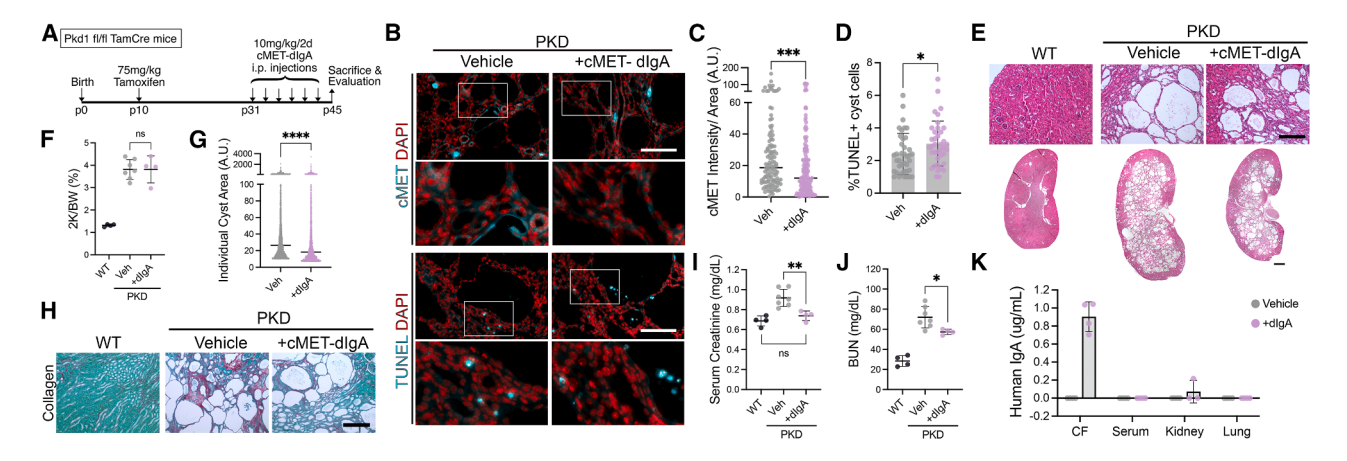


Figure 7. cMET-dlgA treatment prevents cyst expansion in an orthologous Pkd1 mouse model

(A-G) (A) Treatment timeline in tamoxifen-inducible Pkd1 fl/fl mouse model. PKD1 gene excision was induced on p10 followed by single i.p. injections of either 10 mg/kg/2 day cMET-dlgA or vehicle starting at 3 weeks post-induction (p31) for 2 weeks and sacrificed 2 days after the final injection (p45). Analysis of paraffinembedded kidney sections from these mice (n=4) included immunofluorescent staining for (B) cMET or TUNEL (cyan) and DAPI (red), scale bar, 100um; quantification using ImageJ of (C) total cMET fluorescent intensity in cyst cells, median denoted in each group; and (D) TUNEL + cyst cells as a fraction of total nuclei in the cyst; (E) H&E stain-representative images; scale bar, 100 μ m; stitched composite images, scale bar, 1 mm. (F) Two kidney weight as a fraction of total body weight (p45). (G) Quantification of individual cyst areas using ImageJ. Each point represents one cyst; median denoted in each group.

(H–J) (H) Sirius Red Fast Green collagen (red) staining, scale bar, 100 µm; quantification (data not shown) was performed using Adobe Photoshop/grid scoring. Analysis of (I) serum creatinine and (J) blood urea nitrogen (BUN) in serum of WT and PKD (–/+dlgA) mice.

(K) Concentrations of cMET-dlgA recovered on p45 in CF, serum, kidney lysate, and lung lysate via sandwich ELISA specific for human lgA1. See also Figures S3 and S4.

Statistical analyses were performed using Mann-Whitney unpaired one-tailed t test and represented as mean ± SD. A p value of less than 0.05 was considered significant.

DISCUSSION

We have developed a strategy to combine the exquisite molecular target specificity of mAbs with a method to deliver mAbs specifically to renal cysts in PKD.^{5,8} Using this approach, we have shown that concentrations of dlgA in the microgram per milliliter range can be achieved in renal cyst lumens in mice, which far exceeds the 50% effective concentrations of most IgG therapeutic mAbs currently in use. The cMET-dlgA was detected in CF 3 days after a single injection, demonstrating the ability of this engineered mAb to target cyst lumen and remain structurally intact. The current study shows that, even after only 1-2 weeks of treatment in rapidly progressing PKD mouse models, it is possible to slow cyst progression and even ameliorate kidney dysfunction using this dlgA approach. These results also support the role of cMET as a driver of cyst progression. No differences were observed in cMET signaling or kidney function in WT mice treated with cMET-dlgA compared to vehicle, demonstrating the specificity of this drug for diseased kidneys and its effectiveness at targeting signaling pathways from the inside of PKD cysts. Furthermore, the lack of targeting and effect that the cMET-dlgA had on small intestines and lungs show the specificity for this approach to only target mucosal surfaces that upregulate plgR in an injured state-such as PKD cystic epithelial cells.

The limited use of IgA mAbs to date has focused mainly on the heightened ability of IgA antibodies, compared to IgGs, to bind $Fc\alpha RI$ in humans and to activate an immune response via opsonization of cancer cells or pathogens. ^{35–40} The possible antibody-dependent cell-mediated cytotoxic (ADCC) effect of our

dlgA mAb was not explored in the present study as mice do not express $Fc\alpha RI$. While $Fc\alpha RI$ has not been explicitly studied in PKD, it is possible that the efficacy of dlgA therapy in humans could be further enhanced if binding to $Fc\alpha RI$ results in clearance of aberrant cystic epithelial cells as was shown for IgA-stimulated, neutrophil-mediated tumor cell killing. 35 The dramatic induction of apoptosis in cyst-lining cells of dlgA-treated mice observed in this study supports this possibility. Aside from the ADCC properties of IgA, their dominant route of mucosal secretion has started to show therapeutic potential, largely in the context of viral clearance mechanisms. 16,42 Until now, the use of dlgA for targeting cyst-luminal proteins through plgR has been unexplored. The few studies investigating IgA mAbs for cancer therapy often require higher doses or more frequent administration of the mAb to overcome the inherently low serum half-life of IgA. 38,39,43 In contrast to diseases like cancer, where therapeutics with prolonged serum half-lives are often beneficial, this may not apply to PKD. In this context, the unidirectional transport of dlgA into the cyst lumen supports sustained drug accumulation at the target site while minimizing prolonged exposure in non-target tissues. It is also likely that the dlgA can partially avoid Fc immune clearance after transcytosis into enclosed renal cysts as well as avoid degradation from metalloproteases after SC attachment. N-linked glycans have been reported to determine the stability⁴⁴ and blood clearance of human IgA1,45 and modification of these sugars can improve serum pharmacokinetic properties of polymeric IgA molecules by affecting their susceptibility for the carbohydrate-specific, endocytic asialoglycoprotein receptor and the mannose receptor.¹⁵ We did observe apparent heterogeneous glycosylation



patterns on our cMET-dlgA, which was cloned onto the wild-type human lgA1 backbone, producing two molecular weight variants $\sim\!\!450\text{--}500\,$ kDa. Interestingly, it appears that the heavier dlgA species may have trafficked into CF more efficiently than the lighter glycoform, but further investigation is needed to confirm this. Previously, development of certain plgR-binding peptides, heavy chain variable (VHH) fragments, or lgG-J chain conjugates has been pursued in an effort to enhance mucosal trafficking of lgGs or the serum half-life of lgA molecules. While these may be hopeful therapeutic options in the future, the natural affinity of dlgA for plgR far exceeds modified or conjugate proteins 15,51 and would most likely pose a lower immunogenicity risk than a drug with little homology to endogenous proteins.

While concurrent production and testing of our anti-cMET mAb in IgG format was not practical at this early stage in drug development, a direct head-to-head comparison of each isotype's ability to inhibit disease progression while minimizing extra-renal side effects would be of interest in future research. Our lab previously reported that parentally administered IgG was unable to target to CF in multiple mouse models of PKD. Still, IgG mAbs are able to bind the neonatal receptor, FcRn, a bidirectional transporter⁵² found to be expressed in podocytes and proximal tubule cells, among others.⁵³ The major recycling pathway of IgGs brought back into circulation through FcRn is well known. 53,54 However, they can also reportedly be directed to mucosal surfaces via FcRn-mediated transcytosis from the basolateral to apical membrane of polarized intestinal and lung epithelium.^{52,55} While this pathway is not fully understood, it is thought to be a mechanism of immune surveillance at the mucosal surface and subsequent recycling of the IgG mAb back into the interstitium to present major histocompatibility complex antigens to immune cells.⁵⁶ Therefore, we do not believe IgG mAbs are suitable for cyst targeting through FcRn, nor would they have a therapeutic impact on cyst-luminal target proteins for two reasons. First, if IgG was transcytosed into renal cvst lumen via FcRn, which has never been shown in the literature to the best of our knowledge, it is more likely to be degraded or recycled back to the interstitium than to remain in CF as we have shown dlgA does. Second, unlike plgR-mediated dlgA transcytosis, during FcRn-mediated IgG transcytosis, extracellular release of IgG occurs only at a neutral pH⁴⁸ and would therefore not be expected to be released frequently into the acidic CF environment.

The intracellular regulation of cMET has been surprisingly under-studied in PKD even though its intricate role is well characterized in cancer metastasis. ^{57,58} cMET is recognized for triggering protective mechanisms against oxidative damage associated with accelerated growth metabolism, ⁵⁹ a form of damage well documented to play a substantial role in PKD. ^{60,61} Based on the findings from this study, we speculate that, after continuous cMET inhibition, cyst-lining cells lose their capacity to manage escalating oxidative stress resulting from PKD progression, which may lead to halting of cyst growth/proliferation and the eventual induction of cell death of cyst-lining epithelia. Another possibility is that the cMET-dlgA caused RTK ectodomain shedding, ^{31,62} allowing the soluble cMET N-terminal fragment to act as a decoy for HGF binding to other cMET receptors on the cell surface. ^{31,63} Without persistent

HGF signaling during chronic injury, it has been reported that the intracellular role of cMET reverses to become a potent proapoptotic factor in epithelial cells $^{63-65}$; however, this phenomenon has not yet been investigated in PKD. Like cMET, the roles of many other key pathways in PKD pathogenesis remain somewhat elusive yet may hold promise as PKD drug targets. Our antibody-targeting approach has the distinct advantage of allowing numerous pre-existing IgG mAbs—including mAbs that are already in clinical use—to be repurposed, coupling their established ability to potently target a protein of interest with the distinctive ability of dIgA mAbs to reach cyst lumen. Some molecular targets such as the epidermal growth factor receptor, tumor necrosis factor alpha, or transforming growth factor $\beta^{5,32,66}$ may be excellent candidates for our approach based on their known roles in PKD and presence in cyst lumen.

One limitation in employing a model such as the Bpk line for this study is the potential variation in renal plgR expression, as well as dlgA target protein expression, throughout early mouse development and among different tubule types. It is possible that the effect of cMET-dlgA was dampened in these juvenile mice as protein expression levels vary and cyst size changes rapidly during the 1-week treatment window. Variability was also seen in the progression of disease severity in the early-onset tamoxifen-inducible Pkd1 model, potentially affecting efficacy studies as well. Nevertheless, the conclusions from this study were strengthened by the validation of the technique in multiple PKD models. Pharmacokinetic (PK) studies in the Sprague-Dawley Han rat model proved beneficial to investigate dlgA renal trafficking at a stage of cystogenesis where cyst growth has essentially plateaued. This time point minimized confounding parameters that occur in earlier development and cystogenesis. Conversely, the rapid-onset Bpk model allowed for short-term efficacy studies that spanned multiple stages of PKD. Results from the tamoxifen-inducible Pkd1 mouse studies support those from the Bpk studies but demonstrate therapeutic potential in a model orthologous to human PKD.

Until now, the investigation of PKD therapeutics has focused on SM inhibitors against numerous kinases, G protein-coupled receptors, ion channels, and transcription factors. ^{5,66} Our study lays the ground work to investigate a wide range of molecular targets and drug candidates through a biological drug approach in an effort to eliminate off-target effects seen with SM drugs. The versatility of dlgA mAbs could also be applicable for treating other luminal surface diseases where long-term treatment options are limited. For example, in cystic fibrosis, plgR is highly upregulated in lung epithelial cells defective for the cystic fibrosis transmembrane conductance regulator, CFTR, compared to healthy lungs. ^{67,68} This highlights another disease environment where plgR-mediated dlgA mAbs could diversify therapeutic strategies.

Important pharmacokinetic aspects of dlgA-based therapy, such as minimum required dosing frequency and concentration, must still be optimized following this study. Because our cMET-dlgA successfully accumulated in renal CF over multiple days, it is likely that less frequent dosing will be sufficient than the regimen tested here. Infrequent dosing would be extremely beneficial for a human PKD therapeutic considering patients may need to continue treatment over decades. Based on this

Article



study, testing of dlgA mAbs in larger preclinical studies as well as future clinical studies is justified in order to define these parameters further. Bispecific dlgA antibodies may also be explored as an opportunity to expand this mechanism by taking advantage of the four separate antigen-binding domains on dlgA that could be utilized to simultaneously target a wide range of proteins. In conclusion, the data shown here illustrate preclinical proof of therapeutic efficacy for specifically targeting cyst-luminal proteins with recombinant dlgA mAbs. The findings may facilitate further investigations into the development antibody-based therapeutics for PKD and potentially other indications that involve epithelial-enclosed compartments.

Limitations of the study

- Tubule-specific plgR expression across kidney segments or disease stages may influence delivery to cyst lumen and may cause treatment to be more or less effective in certain cyst populations.
- The volume of CF obtained varied widely between individual mice due to technical limitations inherent to current collection methods. The variability in body weight between litters at the developmental stages used in this study also impacted CF recovery volumes. This limited the ability to precisely extrapolate long-term dosing requirements. Future refinements in microsampling or integration of ex vivo dosing models could improve quantification and enhance translational relevance.
- While reductions in cyst burden and inflammatory markers were observed, deeper in vivo mechanistic studies (e.g., cell-specific uptake, effects of heterogeneous glycosylation, or cellular responses to target engagement) would strengthen understanding of drug kinetics.

RESOURCE AVAILABILITY

Lead contact

Requests for further information and resources should be directed to and will be fulfilled by the lead contact and corresponding author, Thomas Weimbs (weimbs@ucsb.edu).

Materials availability

Anti-cMET human IgA₁ HC and LC recombinant plasmids generated in this study have been deposited on Addgene (HC RRID: Addgene_246597; LC RRID: Addgene_246598). The cre-inducible Pkd1^{fl/fl} KO mouse line generated in this study will be made available on request but may require a payment and/or a completed materials transfer agreement.

Data and code availability

- Raw images and in vivo animal data reported in this paper will be shared by the lead contact upon request.
- This paper does not report original code.
- Any additional information required to reanalyze the data reported in this
 paper is available from the lead contact upon request.

ACKNOWLEDGMENTS

This work was supported by grants from the NIH (R01DK109563 and R01DK124895), Chinook Therapeutics, and the US Department of Defense (W81XWH2010827) and gifts from the Amy P. Goldman Foundation and the Lillian Goldman Charitable Trust to the University of California, Santa Barbara, to support the work of T.W. Dr. Stefan Lohse (Universität des Saarlandes, Germany) and Charles Pilette (Université Catholique de Louvain) generously pro-

vided reagents. Dr. Oliver Wessley (Cleveland Clinic) and Dr. Muthusamy Thangaraju (Augusta University) provided PKD animals. We thank Dr. Jacob Torres and Nickolas Holznecht for advice and assistance with rodent experiments, as well as Thomas Evans, Reece Foehr, Tanisha Ram, Aziz Hamza, Sabrina Morales, and Jules Goldstein, for helpful discussions and experimental assistance.

AUTHOR CONTRIBUTIONS

M.F.S. contributed to antibody engineering, production, experimental design, animal procedures, manuscript preparation, and data analysis. B.C.B. and T.C. contributed to antibody engineering, production, and *in vitro* experiments. A.K.S. contributed to antibody purification design and optimization. S.A.P. and Y.L. contributed to experiments and data analysis and quantification. T.W. acted as the principal investigator and contributed to the design and supervision of experiments, the preparation of figures, and writing of the manuscript. All authors contributed to the interpretation of the data, revised the manuscript, and approved the final version.

DECLARATION OF INTERESTS

T.W. is an inventor on issued and pending patents filed by UCSB related to PKD; T.W. is a shareholder and executive of Santa Barbara Nutrients, Inc., was on the scientific advisory board of Chinook Therapeutics, and has received research funding from Chinook Therapeutics and Kyowa Kirin.

STAR*METHODS

Detailed methods are provided in the online version of this paper and include the following:

- KEY RESOURCES TABLE
- EXPERIMENTAL MODEL AND STUDY PARTICIPANT DETAILS
 - o Animals
 - Cell lines
- METHOD DETAILS
 Antibody characterization
 - In vivo antibody treatments
 - Analytical assays
- QUANTIFICATION AND STATISTICAL ANALYSIS
 - Statistics
 - o Histology quantification

SUPPLEMENTAL INFORMATION

Supplemental information can be found online at https://doi.org/10.1016/j.xcrm.2025.102335.

Received: April 21, 2024 Revised: May 27, 2025 Accepted: August 12, 2025 Published: September 5, 2025

REFERENCES

- Bergmann, C., Guay-Woodford, L.M., Harris, P.C., Horie, S., Peters, D.J. M., and Torres, V.E. (2018). Polycystic kidney disease. Nat. Rev. Dis. Primer 4, 50. https://doi.org/10.1038/s41572-018-0047-y.
- Olsan, E.E., West, J.D., Torres, J.A., Doerr, N., and Weimbs, T. (2018). Identification of targets of IL-13 and STAT6 signaling in polycystic kidney disease. Am. J. Physiol. Renal Physiol. 315, F86–F96. https://doi.org/10. 1152/ajprenal.00346.2017.
- Anderson, C.L. (2020). Doubts about the efficacy of tolvaptan for polycystic kidney disease. Clin. Nephrol. 93, 307–309. https://doi.org/10.5414/ CN109927Letter.



- Torres, V.E. (2019). Pro: Tolvaptan delays the progression of autosomal dominant polycystic kidney disease. Nephrol. Dial. Transplant. 34, 30–34. https://doi.org/10.1093/ndt/gfy297.
- Weimbs, T., Shillingford, J.M., Torres, J., Kruger, S.L., and Bourgeois, B.C. (2018). Emerging targeted strategies for the treatment of autosomal dominant polycystic kidney disease. Clin. Kidney J. 11, i27–i38. https://doi.org/10.1093/ckj/sfy089.
- Sliwkowski, M.X., and Mellman, I. (2013). Antibody therapeutics in cancer. Science 341, 1192–1198. https://doi.org/10.1126/science.1241145.
- Dalziel, M., Beers, S.A., Cragg, M.S., and Crispin, M. (2018). Through the barricades: overcoming the barriers to effective antibody-based cancer therapeutics. Glycobiology 28, 697–712. https://doi.org/10. 1093/glycob/cwy043.
- Olsan, E.E., Matsushita, T., Rezaei, M., and Weimbs, T. (2015). Exploitation of the Polymeric Immunoglobulin Receptor for Antibody Targeting to Renal Cyst Lumens in Polycystic Kidney Disease. J. Biol. Chem. 290, 15679–15686. https://doi.org/10.1074/jbc.M114.607929.
- Mostov, K.E., Altschuler, Y., Chapin, S.J., Enrich, C., Low, S.H., Luton, F., Richman-Eisenstat, J., Singer, K.L., Tang, K., and Weimbs, T. (1995).
 Regulation of protein traffic in polarized epithelial cells: the polymeric immunoglobulin receptor model. Cold Spring Harb. Symp. Quant. Biol. 60, 775–781. https://doi.org/10.1101/sqb.1995.060.01.083.
- Turula, H., and Wobus, C.E. (2018). The Role of the Polymeric Immunoglobulin Receptor and Secretory Immunoglobulins during Mucosal Infection and Immunity. Viruses 10, 237. https://doi.org/10.3390/v10050237.
- Kumar Bharathkar, S., Parker, B.W., Malyutin, A.G., Haloi, N., Huey-Tubman, K.E., Tajkhorshid, E., and Stadtmueller, B.M. (2020). The structures of Secretory and dimeric Immunoglobulin A. eLife 9, e56098. https://doi.org/10.7554/eLife.56098.
- Olsan, E.E., Mukherjee, S., Wulkersdorfer, B., Shillingford, J.M., Giovannone, A.J., Todorov, G., Song, X., Pei, Y., and Weimbs, T. (2011). Signal transducer and activator of transcription-6 (STAT6) inhibition suppresses renal cyst growth in polycystic kidney disease. Proc. Natl. Acad. Sci. 108, 18067–18072. https://doi.org/10.1073/pnas.1111966108.
- Burgmaier, K., Buffin-Meyer, B., Klein, J., Becknell, B., McLeod, D., Boeckhaus, J., Gross, O., Dafinger, C., Siwy, J., Decramer, S., et al. (2025). Urinary peptide signature distinguishes autosomal recessive polycystic kidney disease from other causes of chronic kidney disease. Clin. Kidney J. 18, sfaf093. https://doi.org/10.1093/ckj/sfaf093.
- Krawczyk, K.M., Nilsson, H., Nyström, J., Lindgren, D., Leandersson, K., Swärd, K., and Johansson, M.E. (2019). Localization and Regulation of Polymeric Ig Receptor in Healthy and Diseased Human Kidney. Am. J. Pathol. 189, 1933–1944. https://doi.org/10.1016/j.ajpath.2019.06.015.
- Lombana, T.N., Rajan, S., Zorn, J.A., Mandikian, D., Chen, E.C., Estevez, A., Yip, V., Bravo, D.D., Phung, W., Farahi, F., et al. (2019). Production, characterization, and in vivo half-life extension of polymeric IgA molecules in mice. mAbs 11, 1122–1138. https://doi.org/10.1080/19420862.2019. 1622940.
- Robinson, J.K., Blanchard, T.G., Levine, A.D., Emancipator, S.N., and Lamm, M.E. (2001). A Mucosal IgA-Mediated Excretory Immune System In Vivo1. J. Immunol. 166, 3688–3692. https://doi.org/10.4049/jimmunol. 166.6.3688
- Brown, W.R., and Kloppel, T.M. (1989). The liver and IgA: immunological, cell biological and clinical implications. Hepatol. Baltim Md 9, 763–784. https://doi.org/10.1002/hep.1840090518.
- Moldoveanu, Z., Moro, I., Radl, J., Thorpe, S.R., Komiyama, K., and Mestecky, J. (1990). Site of Catabolism of Autologous and Heterologous IgA in Non-Human Primates. Scand. J. Immunol. 32, 577–583. https://doi.org/10.1111/j.1365-3083.1990.tb03199.x.
- Horie, S., Higashihara, E., Nutahara, K., Mikami, Y., Okubo, A., Kano, M., and Kawabe, K. (1994). Mediation of renal cyst formation by hepatocyte growth factor. Lancet Lond. Engl 344, 789–791. https://doi.org/10.1016/ s0140-6736(94)92344-2.

- Qin, S., Taglienti, M., Nauli, S.M., Contrino, L., Takakura, A., Zhou, J., and Kreidberg, J.A. (2010). Failure to ubiquitinate c-Met leads to hyperactivation of mTOR signaling in a mouse model of autosomal dominant polycystic kidney disease. J. Clin. Investig. 120, 3617–3628. https://doi.org/10. 1172/JCI41531.
- Ikeda, K., Kusaba, T., Tomita, A., Watanabe-Uehara, N., Ida, T., Kitani, T., Yamashita, N., Uehara, M., Matoba, S., Yamada, T., and Tamagaki, K. (2020). Diverse Receptor Tyrosine Kinase Phosphorylation in Urine-Derived Tubular Epithelial Cells from Autosomal Dominant Polycystic Kidney Disease Patients. Nephron 144, 525–536. https://doi.org/10.1159/ 000509419.
- Park, H., Kim, D., Kim, E., Sa, J.K., Lee, H.W., Yu, S., Oh, J., Kim, S.H., Yoon, Y., and Nam, D.H. (2017). Tumor Inhibitory Effect of IRCR201, a Novel Cross-Reactive c-Met Antibody Targeting the PSI Domain. Int. J. Mol. Sci. 18, 1968. https://doi.org/10.3390/ijms18091968.
- Prat, M., Oltolina, F., and Basilico, C. (2014). Monoclonal Antibodies against the MET/HGF Receptor and Its Ligand: Multitask Tools with Applications from Basic Research to Therapy. Biomedicines 2, 359–383. https://doi.org/10.3390/biomedicines2040359.
- Bhaskar, V., Goldfine, I.D., Bedinger, D.H., Lau, A., Kuan, H.F., Gross, L.M., Handa, M., Maddux, B.A., Watson, S.R., Zhu, S., et al. (2012). A fully human, allosteric monoclonal antibody that activates the insulin receptor and improves glycemic control. Diabetes 61, 1263–1271. https://doi.org/ 10.2337/db11-1578.
- Low, S.H., Miura, M., Roche, P.A., Valdez, A.C., Mostov, K.E., and Weimbs, T. (2000). Intracellular Redirection of Plasma Membrane Trafficking after Loss of Epithelial Cell Polarity. Mol. Biol. Cell 11, 3045–3060.
- Torres, J.A., Rezaei, M., Broderick, C., Lin, L., Wang, X., Hoppe, B., Cowley, B.D., Jr., Savica, V., Torres, V.E., Khan, S., et al. (2019). Crystal deposition triggers tubule dilation that accelerates cystogenesis in polycystic kidney disease. J. Clin. Investig. 129, 4506–4522. https://doi.org/10.1172/JCl128503.
- Torres, J.A., Kruger, S.L., Broderick, C., Amarlkhagva, T., Agrawal, S., Dodam, J.R., Mrug, M., Lyons, L.A., and Weimbs, T. (2019). Ketosis Ameliorates Renal Cyst Growth in Polycystic Kidney Disease. Cell Metab. 30, 1007–1023.e5. https://doi.org/10.1016/j.cmet.2019.09.012.
- Torres, J.A., Holznecht, N., Asplund, D.A., Amarlkhagva, T., Kroes, B.C., Rebello, J., Agrawal, S., and Weimbs, T. (2024). A combination of β-hydroxybutyrate and citrate ameliorates disease progression in a rat model of polycystic kidney disease. Am. J. Physiol. Renal Physiol. 326, F352– F368. https://doi.org/10.1152/ajprenal.00205.2023.
- Spina, A., De Pasquale, V., Cerulo, G., Cocchiaro, P., Della Morte, R., Avallone, L., and Pavone, L.M. (2015). HGF/c-MET Axis in Tumor Microenvironment and Metastasis Formation. Biomedicines 3, 71–88. https://doi.org/10.3390/biomedicines3010071.
- García-Vilas, J.A., and Medina, M.Á. (2018). Updates on the hepatocyte growth factor/c-Met axis in hepatocellular carcinoma and its therapeutic implications. World J. Gastroenterol. 24, 3695–3708. https://doi.org/10. 3748/wjg.v24.i33.3695.
- Petrelli, A., Circosta, P., Granziero, L., Mazzone, M., Pisacane, A., Fenoglio, S., Comoglio, P.M., and Giordano, S. (2006). Ab-induced ectodomain shedding mediates hepatocyte growth factor receptor down-regulation and hampers biological activity. Proc. Natl. Acad. Sci. USA 103, 5090–5095. https://doi.org/10.1073/pnas.0508156103.
- Formica, C., and Peters, D.J.M. (2020). Molecular pathways involved in injury-repair and ADPKD progression. Cell. Signal. 72, 109648. https://doi.org/10.1016/j.cellsig.2020.109648.
- Fu, Y., Kim, I., Lian, P., Li, A., Zhou, L., Li, C., Liang, D., Coffey, R.J., Ma, J., Zhao, P., et al. (2010). Loss of Bicc1 impairs tubulomorphogenesis of cultured IMCD cells by disrupting E-cadherin-based cell-cell adhesion. Eur. J. Cell Biol. 89, 428–436. https://doi.org/10.1016/j.ejcb.2010.01.002.
- Piontek, K., Menezes, L.F., Garcia-Gonzalez, M.A., Huso, D.L., and Germino, G.G. (2007). A critical developmental switch defines the kinetics of

Article



- kidney cyst formation after loss of Pkd1. Nat. Med. 13, 1490–1495. https://doi.org/10.1038/nm1675.
- Brandsma, A.M., Bondza, S., Evers, M., Koutstaal, R., Nederend, M., Jansen, J.H.M., Rösner, T., Valerius, T., Leusen, J.H.W., and Ten Broeke, T. (2019). Potent Fc Receptor Signaling by IgA Leads to Superior Killing of Cancer Cells by Neutrophils Compared to IgG. Front. Immunol. 10, 704. https://doi.org/10.3389/fimmu.2019.00704.
- Bhaskara, V., Leal, M.T., Seigner, J., Friedrich, T., Kreidl, E., Gadermaier, E., Tesarz, M., Rogalli, A., Stangl, L., Wallwitz, J., et al. (2021). Efficient production of recombinant secretory IgA against Clostridium difficile toxins in CHO-K1 cells. J. Biotechnol. 331, 1–13. https://doi.org/10.1016/j.jbiotec. 2021.02.013.
- Lohse, S., Meyer, S., Meulenbroek, L.A.P.M., Jansen, J.H.M., Nederend, M., Kretschmer, A., Klausz, K., Möginger, U., Derer, S., Rösner, T., et al. (2016). An Anti-EGFR IgA That Displays Improved Pharmacokinetics and Myeloid Effector Cell Engagement In Vivo. Cancer Res. 76, 403–417. https://doi.org/10.1158/0008-5472.CAN-15-1232.
- Meyer, S., Nederend, M., Jansen, J.H.M., Reiding, K.R., Jacobino, S.R., Meeldijk, J., Bovenschen, N., Wuhrer, M., Valerius, T., Ubink, R., et al. (2016). Improved in vivo anti-tumor effects of IgA-Her2 antibodies through half-life extension and serum exposure enhancement by FcRn targeting. mAbs 8, 87–98. https://doi.org/10.1080/19420862.2015.1106658.
- Leusen, J.H.W. (2015). IgA as therapeutic antibody. Mol. Immunol. 68, 35–39. https://doi.org/10.1016/j.molimm.2015.09.005.
- von Gunten, S., Schneider, C., Imamovic, L., and Gorochov, G. (2023).
 Antibody diversity in IVIG: Therapeutic opportunities for novel immunotherapeutic drugs. Front. Immunol. 14, 1166821. https://doi.org/10.3389/fimmu.2023.1166821.
- 41. Bruhns, P., and Jönsson, F. (2015). Mouse and human FcR effector functions. Immunol. Rev. 268, 25–51. https://doi.org/10.1111/imr.12350.
- de Sousa-Pereira, P., and Woof, J.M. (2019). IgA: Structure, Function, and Developability. Antibodies 8, 57. https://doi.org/10.3390/antib8040057.
- Rouwendal, G.J., van der Lee, M.M., Meyer, S., Reiding, K.R., Schouten, J., de Roo, G., Egging, D.F., Leusen, J.H., Boross, P., Wuhrer, M., et al. (2016). A comparison of anti-HER2 IgA and IgG1 in vivo efficacy is facilitated by high N-glycan sialylation of the IgA. mAbs 8, 74–86. https://doi. org/10.1080/19420862.2015.1102812.
- Pan, S., Manabe, N., Ohno, S., Komatsu, S., Fujimura, T., and Yamaguchi, Y. (2024). Each N-glycan on human IgA and J-chain uniquely affects oligomericity and stability. Biochim. Biophys. Acta. Gen. Subj. 1868, 130536. https://doi.org/10.1016/j.bbagen.2023.130536.
- Rifai, A., Fadden, K., Morrison, S.L., and Chintalacharuvu, K.R. (2000). The N-glycans determine the differential blood clearance and hepatic uptake of human immunoglobulin (lg)A1 and IgA2 isotypes. J. Exp. Med. 191, 2171–2182. https://doi.org/10.1084/jem.191.12.2171.
- Borrok, M.J., DiGiandomenico, A., Beyaz, N., Marchetti, G.M., Barnes, A.S., Lekstrom, K.J., Phipps, S.S., McCarthy, M.P., Wu, H., Dall'Acqua, W.F., et al. (2018). Enhancing IgG distribution to lung mucosal tissue improves protective effect of anti–Pseudomonas aeruginosa antibodies. JCI Insight 3, e97844. https://doi.org/10.1172/jci.insight.97844.
- Maruthachalam, B.V., Zwolak, A., Lin-Schmidt, X., Keough, E., Tamot, N., Venkataramani, S., Geist, B., Singh, S., and Ganesan, R. (2020). Discovery and characterization of single-domain antibodies for polymeric Ig receptor-mediated mucosal delivery of biologics. mAbs 12, 1708030. https:// doi.org/10.1080/19420862.2019.1708030.
- Mao, C., Near, R., Shibad, V., Zhong, X., and Gao, W. (2020). An IgA mimicry of IgG that binds Polymeric Immunoglobulin Receptor for mucosa transcytosis. Antib. Ther. 3, 157–162. https://doi.org/10.1093/abt/thae014
- Emmerson, C.D., van der Vlist, E.J., Braam, M.R., Vanlandschoot, P., Merchiers, P., de Haard, H.J.W., Verrips, C.T., van Bergen en Henegouwen, P.M.P., and Dolk, E. (2011). Enhancement of polymeric immunoglob-

- ulin receptor transcytosis by biparatopic VHH. PLoS One 6, e26299. https://doi.org/10.1371/journal.pone.0026299.
- Wang, Q., Chen, Y., Pelletier, M., Cvitkovic, R., Bonnell, J., Chang, C.Y., Koksal, A.C., O'Connor, E., Gao, X., Yu, X.Q., et al. (2017). Enhancement of antibody functions through Fc multiplications. mAbs 9, 393–403. https://doi.org/10.1080/19420862.2017.1281505.
- Johansen, F.E., Braathen, R., and Brandtzaeg, P. (2001). The J Chain Is Essential for Polymeric Ig Receptor-Mediated Epithelial Transport of IgA. J. Immunol. 167, 5185–5192. https://doi.org/10.4049/jimmunol.167. 9.5185.
- Dickinson, B.L. (2016). Unraveling the immunopathogenesis of glomerular disease. Clin. Immunol. 169, 89–97. https://doi.org/10.1016/j.clim.2016. 06.011
- Dylewski, J.F., Haddad, G., and Blaine, J. (2024). Exploiting the neonatal crystallizable fragment receptor to treat kidney disease. Kidney Int. 105, 54–64. https://doi.org/10.1016/j.kint.2023.09.024.
- Blaine, J. (2021). Generating a Podocyte-Specific FcRn Knockout Mouse.
 Methods Mol. Biol. 2224, 123–132. https://doi.org/10.1007/978-1-0716-1008-4_9.
- Tzaban, S., Massol, R.H., Yen, E., Hamman, W., Frank, S.R., Lapierre, L.A., Hansen, S.H., Goldenring, J.R., Blumberg, R.S., and Lencer, W.I. (2009). The recycling and transcytotic pathways for IgG transport by FcRn are distinct and display an inherent polarity. J. Cell Biol. 185, 673–684. https://doi.org/10.1083/jcb.200809122.
- Spiekermann, G.M., Finn, P.W., Ward, E.S., Dumont, J., Dickinson, B.L., Blumberg, R.S., and Lencer, W.I. (2002). Receptor-mediated Immunoglobulin G Transport Across Mucosal Barriers in Adult Life. J. Exp. Med. 196, 303–310. https://doi.org/10.1084/jem.20020400.
- Kim, K.H., and Kim, H. (2017). Progress of antibody-based inhibitors of the HGF-cMET axis in cancer therapy. Exp. Mol. Med. 49, e307. https://doi. org/10.1038/emm.2017.17.
- Barrow-McGee, R., and Kermorgant, S. (2014). Met endosomal signalling: In the right place, at the right time. Int. J. Biochem. Cell Biol. 49, 69–74. https://doi.org/10.1016/j.biocel.2014.01.009.
- Chakraborty, S., Balan, M., Flynn, E., Zurakowski, D., Choueiri, T.K., and Pal, S. (2019). Activation of c-Met in cancer cells mediates growth-promoting signals against oxidative stress through Nrf2-HO-1. Oncogenesis 8, 7. https://doi.org/10.1038/s41389-018-0116-9.
- Pellegrini, H., Sharpe, E.H., Liu, G., Nishiuchi, E., Doerr, N., Kipp, K.R., Chin, T., Schimmel, M.F., and Weimbs, T. (2023). Cleavage fragments of the C-terminal tail of polycystin-1 are regulated by oxidative stress and induce mitochondrial dysfunction. J. Biol. Chem. 299, 105158. https:// doi.org/10.1016/j.jbc.2023.105158.
- Schreiber, R., Buchholz, B., Kraus, A., Schley, G., Scholz, J., Ousingsawat, J., and Kunzelmann, K. (2019). Lipid Peroxidation Drives Renal Cyst Growth In Vitro through Activation of TMEM16A. J. Am. Soc. Nephrol. 30, 228–242. https://doi.org/10.1681/ASN.2018010039.
- Schelter, F., Kobuch, J., Moss, M.L., Becherer, J.D., Comoglio, P.M., Boccaccio, C., and Krüger, A. (2010). A disintegrin and metalloproteinase-10 (ADAM-10) mediates DN30 antibody-induced shedding of the met surface receptor. J. Biol. Chem. 285, 26335–26340. https://doi.org/10.1074/jbc.M110.106435.
- Deheuninck, J., Foveau, B., Goormachtigh, G., Leroy, C., Ji, Z., Tulasne, D., and Fafeur, V. (2008). Caspase cleavage of the MET receptor generates an HGF interfering fragment. Biochem. Biophys. Res. Commun. 367, 573–577. https://doi.org/10.1016/j.bbrc.2007.12.177.
- 64. Lefebvre, J., Muharram, G., Leroy, C., Kherrouche, Z., Montagne, R., Ichim, G., Tauszig-Delamasure, S., Chotteau-Lelievre, A., Brenner, C., Mehlen, P., and Tulasne, D. (2013). Caspase-generated fragment of the Met receptor favors apoptosis via the intrinsic pathway independently of its tyrosine kinase activity. Cell Death Dis. 4, e871. https://doi.org/10.1038/cddis.2013.377.



- Tulasne, D., Deheuninck, J., Lourenco, F.C., Lamballe, F., Ji, Z., Leroy, C., Puchois, E., Moumen, A., Maina, F., Mehlen, P., and Fafeur, V. (2004). Proapoptotic function of the MET tyrosine kinase receptor through caspase cleavage. Mol. Cell Biol. 24, 10328–10339. https://doi.org/10.1128/ MCB.24.23.10328-10339.2004.
- Zhou, X., and Torres, V.E. (2022). Emerging therapies for autosomal dominant polycystic kidney disease with a focus on cAMP signaling. Front. Mol. Biosci. 9, 981963. https://doi.org/10.3389/fmolb.2022.981963.
- de Fays, C., Carlier, F.M., Gohy, S., and Pilette, C. (2022). Secretory Immunoglobulin A Immunity in Chronic Obstructive Respiratory Diseases. Cells 11, 1324. https://doi.org/10.3390/cells11081324.
- Collin, A.M., Lecocq, M., Noel, S., Detry, B., Carlier, F.M., Aboubakar Nana, F., Bouzin, C., Leal, T., Vermeersch, M., De Rose, V., et al. (2020). Lung immunoglobulin A immunity dysregulation in cystic fibrosis. EBioMedicine 60, 102974. https://doi.org/10.1016/j.ebiom.2020.102974.
- Low, S.H., Chapin, S.J., Wimmer, C., Whiteheart, S.W., Kömüves, L.G., Mostov, K.E., and Weimbs, T. (1998). The SNARE Machinery Is Involved in Apical Plasma Membrane Trafficking in MDCK Cells. J. Cell Biol. 141, 1503–1513.

- Tward, A.D., Jones, K.D., Yant, S., Cheung, S.T., Fan, S.T., Chen, X., Kay, M.A., Wang, R., and Bishop, J.M. (2007). Distinct pathways of genomic progression to benign and malignant tumors of the liver. Proc. Natl. Acad. Sci. USA 104, 14771–14776. https://doi.org/10.1073/pnas.0706578104.
- Wrobel, C.N., Debnath, J., Lin, E., Beausoleil, S., Roussel, M.F., and Brugge, J.S. (2004). Autocrine CSF-1R activation promotes Src-dependent disruption of mammary epithelial architecture. J. Cell Biol. 165, 263–273. https://doi.org/10.1083/jcb.200309102.
- Giovannone, A.J., Reales, E., Bhattaram, P., Fraile-Ramos, A., and Weimbs, T. (2018). Tracking Endocytosis and Intracellular Trafficking of Epitope-tagged Syntaxin 3 by Antibody Feeding in Live, Polarized MDCK Cells. Bio. Protoc. 8, e2453. https://doi.org/10.21769/Bio-Protoc.2453.
- Garcia-Castillo, M.D., Lencer, W.I., and Chinnapen, D.J.F. (2018). Transcytosis Assay for Transport of Glycosphingolipids across MDCK-II Cells. Bio. Protoc. 8, e3049. https://doi.org/10.21769/BioProtoc.3049.



STAR*METHODS

KEY RESOURCES TABLE

REAGENT or RESOURCE	SOURCE	IDENTIFIER
Antibodies		
cMET N-terminal	Abcam	Cat#ab51067; RRID: AB_880695
cMET c-terminal	ProSci	Cat#79-590; RRID: AB_2332792
o-cMET (Tyr 1234/1235)	Cell Signaling	Cat#3077; RRID: AB_2143884
oAkt (Thr308)	Cell Signaling	Cat#9275; RRID: AB_329828
o-ERK1/2 (Thr 202/Tyr204)	Cell Signaling	Cat#4370; RRID: AB_2315112
total ERK1/2	Cell Signaling	Cat#4695; RRID: AB_390779
o-Src (Tyr 416)	Cell Signaling	Cat#6943; RRID: AB_10013641
otal Src	Cell Signaling	Cat#2109; RRID: AB_2106059
o-AMPK (Thr 172)	Cell Signaling	Cat#2535; RRID: AB_331250
anti-human IgA, HRP conjugate	Invitrogen	Cat#A18787; RRID: AB_2535564
anti-human IgA, FITC conjugate	Invitrogen	Cat#A18788; RRID: AB_2535565
anti-human IgA, unconjugated	Invitrogen	Cat# A18789; RRID: AB_2535566
peta-actin	Sigma-Aldrich	Cat# A5441; RRID: AB_476744
olgR	R&D Systems	Cat#AF2800; RRID: AB_2283871
AQP1 (B-11)	Santa Cruz Biotechnology	Cat#sc-25287; RRID: AB_626694
mouse Ki67	EMD Millipore	Cat#AB9260; RRID: AB_2142366
rat Ki67	Thermo Fisher	Cat#14-5698-80; RRID: AB_10853185
LTL-FITC	Vector Labs	Cat#FL-1321; RRID: AB_2336559
goat anti-rabbit IgG-biotin	EMD Millipore	Cat#AP132B; RRID: AB_92488
goat anti-rabbit IgG-Texas Red	Invitrogen	Cat#A11012; RRID: AB_2534079
abbit anti-human IgA (alpha chain)-biotin	Abcam	Cat#ab97218; RRID: AB_10681073
streptavidin-HRP	BD Pharmingen	Cat#554066; RRID: AB_2868972
purified polyclonal human dlgA	Charles Pilette, Université Catholique de Louvain	N/A
cMET-dlgA (mouse lgA)	This paper	N/A
cMET-dlgA (human lgA1)	This paper	Heavy chain RRID: Addgene_246597; LC RRID: Addgene_246598
Chemicals, peptides, and recombinant prote	eins	
Freestyle 293 Expression Media containing	Gibco	Cat#12338018
Glutamax		
polyethylenimine, linear (MW 25000)	Polysciences	Cat#23966-100
mouse HGF, carrier free	eBioscience	Cat#14-8431-80
capmatinib/INC280	SelleckChem	Cat#S2788
Critical commercial assays		
DeadEnd fluorometric TUNEL system	Promega	Cat#G3250
QuantiChrom creatinine assay kit	BioAssay Systems	Cat#DICT-500
QuantiChrom urea assay kit	BioAssay Systems	Cat#DIUR-100
Experimental models: Cell lines		
Human: Freestyle 293-F	Gibco	Cat#R79007; RRID: CVCL_D603
Hamster: CHO	ATCC	CCL-61; RRID: CVCL_0214
Dog: MDCK strain II	Low et al. ⁶⁹	N/A
Dog: MDCK stably expressing WT-plgR	Low et al. ⁶⁹	N/A
Mouse: mIMCD-3	ATCC	CRL-2123; RRID: CVCL_0429
Human: HeLa	ATCC	CCL-2; RRID: CVCL_0030

(Continued on next page)



Continued		
REAGENT or RESOURCE	SOURCE	IDENTIFIER
Experimental models: Organisms/strains		
Mouse: Bpk/Bpk, on a C57/Bl6 genetic background	Oliver Wessely, Cleveland Clinic	N/A
Rat: Han:SPRD	Benjamin Cowley, University of Oklahoma Health Sciences Center	N/A
Mouse: Pkd1 ^{fl/+} ERT2-cre [±]	Muthusamy Thangaraju, Augusta University	N/A
Mouse: cre-inducible Pkd1 ^{fl/fl}	This paper	N/A
Recombinant DNA		
pFUSEss-CHIg-hA1	Invivogen	pfusess-hca1
pFUSE2ss-CLlg-hk	Invivogen	pfusess2-hclk
cDNA for anti cMET heavy/light chain Fab regions	IDT	gBlocks gene fragments
pT3-EF1aH c-Met	Tward et al. ⁷⁰	Addgene Plasmid #86498; RRID: Addgene_86498
pIRESpuro3 JCHAIN-myc-His	Stefan Lohse, Universität des Saarlandes	N/A
pCMV3 rat c-MET/HGFR expression vector	Sino Biological	Cat#RG80004-UT
pBabe puro c-met WT	Wrobel et al. ⁷¹	Addgene Plasmid #17493; RRID: Addgene_17493
Software and algorithms		
ImageJ	NIH	https://imagej.net/ij/
CellProfiler	Broad Institute	https://cellprofiler.org/releases
Prism9	GraphPad Software	https://www.graphpad.com
Other		
Vivaflow 200 filtration cassettes, 100kDa MWCOSartorius		Cat#VF20H4

EXPERIMENTAL MODEL AND STUDY PARTICIPANT DETAILS

Animals

All rat and mouse studies adhered to the rules and regulations of the National Institutes of Health with approval of the Institutional Animal Care and Use Committee of the University of California, Santa Barbara. All animals were housed in the animal resource center at the University of California Santa Barbara using a 12-h light/dark cycle at 74°F with *ad libitum* access to food, water, and enrichment. Animals were housed with littermates in groups between 2 and 4 (rats) or 4–6 (mice) without regard to genotype, resulting in a random distribution of PKD and wild-type animals in cohorts. Animals were anesthetized using a combination of 200mg;20mg/kg ketamine:xylazine, followed by cervical dislocation before tissue removal. Tissue samples were snap-frozen in liquid nitrogen following removal for later analysis. Serum samples were collected via cardiac puncture, transferred to a Microtainer tube (Cat#B-D365967; BD), separated by centrifugation, and snap-frozen in liquid nitrogen. Cyst fluid was collected by needle aspiration or by mechanical draining to create "depleted kidney" samples. Animals were sacrificed at ~3p.m. for experimental consistency. The lead researcher was not blinded to the genotypes of animals in treatment groups. Researchers performing daily maintenance were not aware of experimental genotypes.

Mice

The Bpk/Bpk mouse strain, on a C57/Bl6 genetic background, was provided by Oliver Wessely (Cleveland Clinic). Bpk -/- (PKD phenotype) and Bpk +/+ (wt) mice used in this study were generated by breeding two heterozygote parents (wt phenotype). Pkd1^{fl/+} ERT2-cre^{+/-} mice were provided by Dr. Muthusamy Thangaraju (Augusta University). These mice were then bred to produce the cre-inducible Pkd1^{fl/fl} ERT2-cre^{+/+} KO mice used in this study. Equal numbers of males and females were used for all mouse studies. See *In vivo antibody treatments* section for more details.

Rats

Han:SPRD (Anks6 mutant, Cy/+) rats were originally obtained from the University of Oklahoma Health Sciences Center, courtesy of Dr. Benjamin Cowley. Rats were weaned at postnatal day 21, separated by sex, group housed, and randomly assorted into treatment groups with littermate controls. Equal number of male and female adult rats, between 8 and 10 weeks old, were used in this study. See *In vivo antibody treatments* section for more details.

Article



Cell lines

HEK293-F suspension cells were grown in 1L culture flasks and maintained in serum-free Freestyle 293 Expression Media containing Glutamax and 1% penicillin/streptomycin at \sim 135 rpm, 6% CO2, 37°C. mIMCD-3 and CHO cells were grown on 10cm dishes in DMEM-F12 media supplemented with 10% FBS, 1% L-glutamine, and 1% penicillin/streptomycin at 5% CO2, 37°C. MDCK cells were grown on 10cm dishes in MEM media supplemented with 5% FBS, 1% L-glutamine, and 1% penicillin/streptomycin at 5% CO2, 37°C. HeLa cells were grown on 10cm dishes in DMEM media supplemented with 10% FBS, 1% L-glutamine, and 1% penicillin/streptomycin at 5% CO2, 37°C.

METHOD DETAILS

Antibody characterization

Dimeric IgA production

Gene blocks encoding cMET H&L Fab sequences, obtained from U.S. patent ID US20140370022A1, were cloned onto pFUSEss-CHlg-hA1 for heavy chain (HC) or pFUSE2ss-CLlg-hk for light chain (LC) (Invivogen) to produce the final human alpha HC (RRID: Addgene_246597) and kappa LC (RRID: Addgene_246598) expresison plasmids. Human J chain (JC) plasmid, pIRESpuro3 JCHAIN-myc-His, was generously provided by Stefan Lohse (Universität des Saarlandes, Germany). JC plasmid is selectable in E.coli with ampicillin; HC with Zeocin, and LC with blasticidin. HEK293-F cells concentrated to 20×10^6 cells/mL in serum-free Freestyle 293 Expression Media containing Glutamax (Gibco) (no penicillin/streptomycin) were transiently co-transfected with the 3 cMET-dlgA plasmids using linear PEI MW 25000 (Polysciences). These high density transfections were incubated for 4 h in 125mL vented cap culture flasks at \sim 160 rpm, 6% CO2, 37°C. After 4 h, the transfected culture was diluted to 1 \times 10⁶ cells/mL in serum-free Freestyle 293 Expression Media containing Glutamax and 1% penicillin/streptomycin in 1L vented cap culture flasks. dlgA-expressing cultures were maintained for 5–7 days at \sim 135 rpm, 6% CO2, 37°C. Reaction volumes were typically: 25mL transfection culture containing 625 μ g total plasmid DNA in a 150mL flask (20 \times 10⁶ cells/mL), expanded into a 500mL expression culture (1 \times 10⁶ cells/mL) in a 1L flask.

Supernatants were centrifuged, filtered through 0.22 µm PES membranes, and concentrated (10–25×) with 100K MWCO Vivaflow filtration units (Sartorius). dlgA purification utilized Ni-NTA resin (Thermo Fisher, cat#: 88221) for gravity-flow nickel immobilized metal affinity chromatography to remove monomeric IgA followed by anion exchange using a 1mL HiTrap Q column (Cytiva, cat#: 17115301). Fractions containing pure dlgA were pooled together and dialyzed into PBS, pH 7.4.

In vitro functional assays

Specific target binding of the cMET-dIgA was verified in CHO cells grown on poly L-lysine-coated coverslips, transiently transfected with one of the following plasmids: pT3-EF1aH human cMET⁷⁰ gifted by Xin Chen (Addgene plasmid # 86498), pCMV3 rat cMET (SinoBiological, plasmid # RG80004-UT), pcDNA3 mMET-FLAG⁷¹ gifted by Joan Brugge (Addgene plasmid # 17493), or an empty vector for control. Once allowed to express cMET for 48 h, cells were fixed to coverslips with 10% NBF and permeabilized with saponin. Slides were co-stained with the c-MET-dIgA followed by a FITC-conjugated secondary against human IgA, as well as a commercial cMET IgG primary antibody (Abcam, cat#: ab51067), that recognizes all 3 species of cMET followed by an anti-rabbit IgG-Texas Red secondary. For antagonist assays, cells were grown to 80% confluency and serum starved for 5 h, then treated with increasing concentrations of dIgA (0.1–13.5 μ g/mL) for 1 h. Without changing the media, 100ng/mL mouse HGF (carrier free, Cell Signaling) was added to the cells for 15min. Capmatinib/INC280 (SelleckChem) was used as a control. Cell were then lysed in SDS for analysis.

Transcytosis assays

The ability of the cMET-dlgA to cross epithelial barriers was measured using transcytosis assay protocols adapted from previous literature. 69,72,73 Briefly, MDCK cells stably transfected with or without plgR 69 were seeded at 1 million cells/mL in 0.4 μ m Transwell filters (Corning) in 12 well plates and grown into a monolayer in MEM +5% FBS. 500 μ L of basolateral media containing 50 μ g/mL cMET-dlgA in serum free MEM supplemented with 1% defatted-BSA was applied to the basolateral compartment. Transwells were washed and the apical compartment was replaced with serum-free MEM supplemented with 0.06% defatted-BSA. Supernatant samples were collected from the apical compartment after 0, 1, and 24h and analyzed by immunoblot for human IgA. 5ng of cMET-dlgA was loaded alongside the experimental samples for comparison of the size shift that occurs from secretory-component attachment, as well as to estimate transcytosis efficiency.

In vivo antibody treatments

cMET-dlgA was prepared in PBS, pH 7.4 and sterile filtered with a 0.22μm syringe filter. The vehicle (PBS, pH 7.4) was prepared and injected in the same manner as the mAb. For all studies, approximately equal numbers of animals from each litter were treated via intraperitoneal (i.p.) injection with PBS vehicle and dlgA, allowing for analysis of reliable litter-mate controls.

Single injection studies

10 week old Han rats were i.p. injected with 1mg cMET-dlgA or vehicle and euthanized 24 h post-injection. Bpk mice were i.p. injected with 20mg/kg cMET-dlgA or vehicle and analyzed at varied lengths of time post-injection; all were euthanized no later than postnatal day 14. (For example, a pup that was analyzed "3 days post-injection" would have received a single cMET-dlgA injection on postnatal day 11.)



Repeated injection studies

For studies in the Bpk mice detailed in Figures 5 and 6, nursing WT and KO pups were treated with 20mg/kg/day cMET-dlgA or vehicle via i.p. injection for 1 week, starting on postnatal day 7. For studies in the Pkd1^{fl/fl} mice detailed in Figure 7, Pkd1 deletion was induced with a single i.p. dose of 75mg/kg tamoxifen in corn oil on postnatal day 10. KO mice were subsequently treated with 10mg/kg/2d cMET-dlgA or vehicle for 2 weeks starting 3 weeks post-induction and euthanized two days after the final injection.

Analytical assays Human IgA ELISA

To measure recovery of dlgA *in vivo*, sandwich ELISAs were conducted by coating 96-well plates with 2 μg/mL antibody against human lgA (H&L chains, unconjugated, Invitrogen, cat#: A18789), followed by incubation with either CF, serum, TX-100 whole kidney lysates, or TX-100 whole lung lysates from vehicle and dlgA treated mice for 2 h at room temperature. cMET-dlgA from each sample was then incubated with a biotinylated anti-human lgA (heavy chain) capture antibody (Abcam cat#: ab97218), followed by streptavidin-HRP (BD Biosciences cat#: 554066) and detection using TMB colorimetric substrate (Thermo Fisher) at 450nm. A titration of non-specific human dlgA, provided by Charles Pilette from the Université Catholique de Louvain, loaded on the same plate as experimental samples was used as a control and for quantification. To calculate the fraction of cMET-dlgA present in CF relative to the dose given, it was assumed that on average 0.5-1mL total of CF can be recovered from the kidneys of one Bpk juvenile mouse.

Immunoblotting

Tissue preparation and loading has been described previously. 8,26 Briefly, tissues were snap frozen in liquid nitrogen at the time of collection and then homogenized with a Dounce homogenizer in RIPA lysis buffer for dlgA detection or SDS lysis buffer for intracellular protein analysis. Protein concentrations were estimated using the Pierce BCA Protein Assay kit (Thermo Fisher, cat#: Pl23227) and lysates were loaded at 5mg/mL total protein. Serum and CF samples were equalized by loading the same volume for each sample mixed in 2xSDS sample buffer. To observe the cMET-dlgA in its fully assembled form, samples were loaded on a 6% nonreducing SDS-PAGE gel and transferred to a nitrocellulose membrane before HRP detection.

Histology & immunostaining

Formalin-fixed, paraffin-embedded (FFPE) tissues were sectioned (5 μm) and processed for hematoxylin and eosin, immunofluorescence (IF), or immunohistochemistry (IHC) staining as described previously. ²⁶ Small intestines were perfused with 10% neutral buffered formalin prior to overnight fixation and paraffin-embedding. To detect the cMET-dlgA via immunofluorescence, antigens were retrieved in 10 mM citrate-Na at pH 6.0 for 10min in a 95-100C water bath, blocked in serum-free TBST buffer with 0.1% fish skin gelatin, incubated in primary antibody overnight, followed by 0.1% Sudan Black treatment and incubation with a FITC-conjugated secondary. Slides were mounted with ProLong Gold antifade mounting medium after staining for nuclei with DAPI (Thermo Fisher). For immunohistochemical analysis, slides were developed using DAB peroxidase substrate (Vector Cat#: SK-4100), followed by counterstaining with hematoxylin in some cases. Collagen was stained with 0.1% Sirius Red 0.04% Fast Green in picric acid for 4 h at room temperature. Apoptosis was measured using the DeadEnd Fluorometric TUNEL system (Promega, cat#: G3250).

Serum analysis

Serum creatinine was measured with 15 μ L serum per mouse using the QuantiChrom Creatinine Assay Kit (BioAssay Systems, cat# DICT-500). BUN was analyzed with 5 μ L serum per mouse using the QuantiChrom Urea Assay Kit (BioAssay Systems, cat# DIUR-100). Purified creatinine and urea were used as standards in each assays and their optical densities were read at 492nm and 520nm, respectively.

QUANTIFICATION AND STATISTICAL ANALYSIS

Statistics

Researchers performing quantification were blinded and provided animal ID numbers without knowledge of specific treatments. Statistical analyses were performed using Mann-Whitney unpaired one-tailed t-test using Prism9 (GraphPad) software. A p value of less than 0.05 was considered significant. All graph data is represented as mean \pm SEM, unless specified otherwise. Sample sizes were chosen based on experience with previous studies with PKD animals in our lab. In analyses that use fewer than the entire group of experimental animals, animals were chosen randomly for inclusion in the analysis. A minimum of 4 experimental replicates were used for all experiments. Multiple litters were used for each experimental condition tested to avoid potential litter biases.

Histology quantification

Cystic area

Full kidney sections were created from $40\times$ stitched images, and cysts were counted using the analyze particle feature in FIJI (ImageJ). Images were modified with the threshold function, and the total white space was counted and divided by the total kidney area to determine the cystic area. Manual determination of inclusive areas was used to exclude artifacts from tissue sectioning.

Article



Fibrosis

Sirius red-stained sections were imaged at 20× magnification for quantification. Ten images from cortical regions were taken from each kidney. Using Photoshop (Adobe), a grid was placed over each image, and intersections with Sirius red stain were counted as positive, with intersections overlaid on negative space or outside of tissue excluded from the total number of potential intersections.

Immunofluorescent staining

Stained sections were imaged at 20–40× magnification for quantification. Ten images from cortical regions (unless otherwise specified) were taken from each kidney. Cell number was determined with DAPI positive images using FIJI (ImageJ) to automate cell counting. Signal-positive cells were quantified either through an automated Cell Profiler pipeline, or manually counted and classified by location as interstitial (existing outside of tubules and cysts), tubular (existing in cyst-lining cells or healthy epithelial cells), or luminal (inside cyst lumen). The number of positive cells from all ten images was divided by the total number of cells counted to obtain the percentage of signal-positive cells.